Cooperative Shape-Translation Estimation and Control for Time-Varying Linear Formation

Xiaozhen Zhang, Qingkai Yang, *Member, IEEE,* Xianlin Zeng, *Member, IEEE,* Hao Fang, *Member, IEEE,* and Jie Chen, *Fellow, IEEE*

***Abstract*— This paper investigates the time-varying formation control problem of multi-agent systems. A novel leader-follower formation architecture is proposed, termed "linear formation control". In this architecture, both the shape of the formation and its translational motions are represented by a linear transformation matrix determined by the positions of the leaders. This setup allows the leaders' movements to generate time-varying desired formations. To facilitate followers' tracking of desired formations, an integrated control structure is proposed, comprising two estimators and a compatible controller. The first estimator is responsible for obtaining the time-varying linear formation shape parameters by measuring the leaders' relative displacements, the kernel of which essentially involves solving a system of time-varying linear equations in a distributed manner. The second estimator focuses on inferring the time-varying translation parameters using leaders' positions. Subsequently, utilizing the outputs of these estimators, a tracking controller is proposed to track the desired time-varying formation precisely. Finally, the effectiveness of the proposed estimation and control schemes is demonstrated through simulations.**

***Index Terms*— Time-varying formation control, cooperative estimation, time-varying linear equations, multi-agent systems.**

I. Introduction

In collaborative tasks, the behavior of multi-agent systems is often expected to be cohesive. Formation control serves as a unified protocol to coordinate interactions among agents for achieving collaborative objectives. For example, formation control has important applications in cooperative encirclement [1], cooperative transportation [2], [3], agricultural operations [4], and cloud seeding operations [5]. These diverse applications owe their success to the ongoing development of formation control technology.

This work was supported in part by the NSFC under grant 62373048, in part by the National Key Research and Development Program of China under No. 2022YFB4702000, No. 2022YFA1004703, in part by the NSFC under Grants 62133002, U1913602, 62088101, in part by the Fundamental Research Funds for the Central Universities and in part by the Shanghai Municipal Science and Technology Major Project (2021SHZDZX0100). *(Corresponding author: Qingkai Yang.)*

Xiaozhen Zhang, Qingkai Yang, Xianlin Zeng, and Hao Fang are with the National Key Laboratory of Autonomous Intelligent Unmanned Systems, School of Automation, Beijing Institute of Technology, Beijing 100081, China (e-mail: jiaozhen@mail.nwpu.edu.cn, qingkai.yang@bit.edu.cn, xianlin.zeng@bit.edu.cn, fangh@bit.edu.cn).

Jie Chen is with the College of Electronics and Information Engineering, Tongji University, Shanghai 200092, China (e-mail: chenjie@bit.edu.cn).

Inspired by the consensus problem [6], early distributed formation control methods are devised to enable agents to reach a predefined formation at a predetermined location (see, e.g, [7], [8]). The formation shape can be represented by some predefined parameters. For example, a positive value can govern the scale size of formations (see, e.g., [9], [10]). Combining scale with rotation parameters, formation scaling and rotation can be simultaneously achieved (see, e.g., [11], [12]). Since scaling and rotation represent specific types of affine transformation motion, the affine formation control approach employs a square matrix to govern the formation shape that enables more types of formation variations, including shear, reflection, and more (see, e.g., [13]–[15]). However, despite these parameterized formation methods offering a wide range of feasible formation variations, limited attention has been given to the intermediate switching states between two formations during the transformation. This is because many studies (see, e.g., [9], [16]) often involve abrupt step changes in achieving formation transformations. Consequently, there is a need for more comprehensive investigations into time-varying formation control technology to achieve smoother formation variations.

Time-varying formation control provides smooth trajectories when formation switches. It is especially suitable for formation transformation and maneuvering in complex environments. Distributed time-varying formation tracking control schemes are designed in [17], [18], with assuming complete knowledge of both the formation and its derivative information. When the derivative of the desired formation is unknown, signum functions can be used to achieve precisely time-varying formation tracking (see, e.g., [19], [20]). Model uncertainties and external disturbance are further covered in [21] by involving radial basis function neural networks (RBFNNs). As for time-varying formation shape variations, a centralized method is proposed in [22], where scaling and rotation motions can be achieved by manipulating the complex-Laplacian matrix associated with the underlying graph. In time-varying affine formation maneuver, when leaders are with constant velocities, proportional-integral (PI) type control laws are developed under both undirected [13], [23] and directed [24] graphs. As for leaders with time-varying velocities, a distributed control law for solving the formation tracking problem is introduced in [14], where neighboring agents' control inputs are required. This controller is further studied for triple integrator systems [25]. Moreover, the neighbors' inputs are replaced by their

historical information in [26], but where only bounded position error can be achieved. Without neighbors' inputs, the methods proposed in [27] can achieve precise time-varying formation tracking by employing signum functions, which, however, also brings jitters into control input signals. In summary, most leader-follower time-varying formation control methods typically rely on global information about the desired dynamic formation, but it is usually known only to a few leaders (see, e.g., [7], [9], [13], [19]). The unavailability of this global formation information to the followers results in challenges related to formation stabilization and tracking. However, this global desired formation information is implied in the relative displacements of leaders. Therefore, it is possible to employ distributed estimation techniques to extract key information embedded in these relative displacements.

In [28], distributed estimators are introduced to obtain the leader's time-varying trajectory as the feedforward in formation tracking controllers. It is shown that information pertaining to the desired scaling size and overall rotation can also be implicitly found in formation edges (see e.g., [9], [16]). Distributed estimators are proposed for both constant [29] and time-varying [30] formation scale parameters. For planar formations, an estimator capable of simultaneously estimating scale size and rotation parameters is presented in [16] under the framework of affine formation control. A notable aspect of estimating rotation and scaling parameters is that such information can be fully contained within a single edge (a pair of agents). However, when estimated parameters become complex, an edge may only contain a portion of the desired parameter information. For example, the affine transformation matrix parameter that determines the formation shape in the affine formation control approach. In the d-dimensional space, it is known that the affine transformation matrix parameter is determined by at least $d+1$ agents (i.e., d edges) [13]. This indicates that achieving a comprehensive affine formation parameters measurement requires gathering information from multiple edges, thereby forming a system of linear equations. This complex relationship brings challenges in the estimation of intricate formation parameters.

In the past decade, some distributed algorithms for solving the time-invariance system of linear equations have been proposed. For cases with a unique solution, a projected consensus algorithm is introduced in [31] that can enforce each agent's local solution to reach consensus by moving along the tangent space of the corresponding local linear sub-equation. Then, the projected consensus algorithm is extended to arbitrarily initial values in [32], by adding a term that can track the local manifold corresponding to the local linear sub-equation. Furthermore, switching [33] and random [34] networks are also studied in this problem. For time-invariant underdetermined system of linear equations that has multiple solutions, minimum l_1-norm solution, and minimum l_2-norm solution to a prescribed point are studied in [35] and [36], respectively. The time-invariant overdetermined system of linear equations that has redundant row conditions is usually unsolvable, but its least squares solution always exists. Discrete-time [37] and continuous-time [38] distributed algorithms are introduced. A distributed version of Arrow-Hurwicz-Uzawa flow is proposed in [39] derived from the classical centralized form. Although the distributed solution of the time-invariant linear equation has been widely studied in the past several years, there is a lack of research on the distributed solution of a system of time-varying linear equations.

This paper studies the time-varying linear formation control problem of multi-agent systems. The proposed linear formation control method enables more parameters than the affine manner to describe the formation shape, providing a broader flexible formation set for complex maneuver tasks. In the linear formation control method, it is important to note that the overall formation is governed by a time-varying linear transformation matrix, which can be determined by the positions of the leaders. An integrated leader-follower control architecture is proposed for addressing followers' time-varying linear formation tracking problem. First, a distributed estimator are proposed to estimate these time-varying formation shape parameters through collaborative observation of leaders. The essence of this estimator involves solving a system of time-varying linear equations in a distributed manner, expressed as $\mathbf{A}(t)\boldsymbol{x}(t)=\boldsymbol{b}(t)$. Second, a distributed estimator is derived to obtain the time-varying formation translation parameters by observing leaders' positions. Third, using the outputs of those estimators, a formation control law is developed for time-varying linear formation tracking. Finally, an optimization-based linear formation design method is introduced that cascades the proposed time-varying formation architecture to achieve flexible formation variations.

In summary, the main contributions of this paper are given as follows.

1) A new distributed leader-follower formation method, termed linear formation control, is proposed. In this method, the desired formation is represented by a linear transformation matrix determined by leaders' positions. It allows the multi-agent system to perform broader range of formation variations than translation [7], scaling [10], and affine [13] transformations.
2) Time-varying formation maneuvers are considered in this paper. Moreover, the proposed formation control schemes are also applicable to time-varying nominal configuration, which is more challenging than studies on time-invariant nominal configurations in most transformation-based formation control approaches (see, e.g., [9], [14]).
3) The challenge of cooperatively identifying time-varying linear formation parameters is reformulated as the problem of solving a system of time-varying linear equations in a distributed manner. The proposed method requires less dynamic feedforwards than the previous work [40].

The remainder of this paper is organized as follows. First, some preliminaries are given in Section II. Time-varying linear formation control architecture is proposed in Section III, where we also address our primary control objective. Then, two estimators are proposed in Section IV and Section V to estimate time-varying formation shape and translation, respectively. On the basis of the estimated formation parameters, a time-varying linear formation tracking method is devised in Section VI. Next, a simulation of time-varying linear formation

is presented in Section VII. The last section concludes this paper.

II. Preliminaries

This section presents some notations and preliminary results that will be used in this paper.

A. Notations

The operator $\otimes$ stands for the Kronecker product for matrices. Denote the identity matrix with dimension n by $\mathbf{I}_n$. We use $\boldsymbol{1}_n$ and $\boldsymbol{0}_n$ to represents the all-one vector $\begin{bmatrix}1 & \dots & 1\end{bmatrix}^{\mathrm{T}} \in \mathbb{R}^n$ and all-zero vector $\begin{bmatrix}0 & \dots & 0\end{bmatrix}^{\mathrm{T}} \in \mathbb{R}^n$, respectively. For a vector $\boldsymbol{y} \in \mathbb{R}^n$, $\|\boldsymbol{y}\|_1$ denotes the l_1-norm of vector $\boldsymbol{y}$. For a matrix $\mathbf{F} \in \mathbb{R}^{m\times n}$, $\|\mathbf{F}\|_\infty$, $\mathbf{F}^+$, and $\mathrm{rank}\,(\mathbf{F})$ denote the ∞-norm, Moore-Penrose inverse[1], and rank of the matrix $\mathbf{F}$, respectively. The vectorization of $\mathbf{F}$ is represented by $\mathrm{vec}\,(\mathbf{F}) = \left[\boldsymbol{f}_1^{\mathrm{T}}, ..., \boldsymbol{f}_n^{\mathrm{T}}\right]^{\mathrm{T}}$, where $\boldsymbol{f}_i$ denotes the ith column of $\mathbf{F}$. A block-diagonal matrix is represented by $\mathrm{diag}\,\{...\}$. The symbol $\mathrm{vec}\,(\cdot)$ means the vectorization of a matrix. Denote the second smallest eigenvalue of a matrix by $\lambda_2\,(\cdot)$. For vectors $\boldsymbol{p}_1, ..., \boldsymbol{p}_n$, $\mathrm{span}\,\{\boldsymbol{p}_1, ..., \boldsymbol{p}_n\}$ is used to denote the linear span of these vectors. Let $\mathrm{sgn}\,(\cdot)$ denote the signum function. For a vector $\boldsymbol{z} \in \mathbb{R}^n$, $\mathrm{sgn}\,(\boldsymbol{z}) = \begin{bmatrix}\mathrm{sgn}\,(z_1) & \cdots & \mathrm{sgn}\,(z_n)\end{bmatrix}^{\mathrm{T}}$. For $c > 0$ and a closed set $\boldsymbol{\Gamma}$, $\boldsymbol{\mathcal{B}}_c := \{\boldsymbol{x} \in \mathbb{R}^n : \|\boldsymbol{x}\|_{\boldsymbol{\Gamma}} < c\}$, where $\|\boldsymbol{x}\|_{\boldsymbol{\Gamma}} = \inf_{\boldsymbol{y}\in\boldsymbol{\Gamma}} \|\boldsymbol{x} - \boldsymbol{y}\|_2$ is the point-to-set distance from $\boldsymbol{x}$ to $\boldsymbol{\Gamma}$.

B. Graph Theory [42], [43]

A directed graph $\boldsymbol{\mathcal{G}}$ is a pair $(\boldsymbol{\mathcal{V}}, \boldsymbol{\mathcal{E}})$, where $\boldsymbol{\mathcal{V}} = \{v_1, ..., v_n\}$ is a non-empty finite set of nodes and $\boldsymbol{\mathcal{E}} \subseteq \boldsymbol{\mathcal{V}} \times \boldsymbol{\mathcal{V}}$ is a set of ordered pairs of nodes, called edges. An edge (v_j, v_i) represents the communication path from node v_j to node v_i.

The Laplacian matrix $\boldsymbol{\mathcal{L}} \in \mathbb{R}^{n\times n}$ is defined as

$$[\boldsymbol{\mathcal{L}}]_{ij} = \begin{cases} 0 & (v_j, v_i) \notin \boldsymbol{\mathcal{E}} \\ -1 & (v_j, v_i) \in \boldsymbol{\mathcal{E}} \\ -\sum_{j\in\boldsymbol{\mathcal{N}}_i} [\boldsymbol{\mathcal{L}}]_{ij} & i = j \end{cases},$$

where $\boldsymbol{\mathcal{N}}_i = \{j \in \boldsymbol{\mathcal{V}} : \ (v_j, v_i) \in \boldsymbol{\mathcal{E}}\}$ is a set containing all neighbors of node v_i. For an undirected connected graph, the Laplacian matrix is positive semi-definite and has only one zero eigenvalue.

C. Solutions of A System of Linear Equations [44]

A system of linear equations can be written in the following form

$$\mathbf{A}\boldsymbol{x} = \boldsymbol{b}, \tag{1}$$

where $\mathbf{A} \in \mathbb{R}^{r\times c}$, $\boldsymbol{b} \in \mathbb{R}^r$, $\boldsymbol{x} \in \mathbb{R}^c$. The solutions of the system of linear equations (1) are identified based on the rank conditions of $\mathbf{A}$ and $\boldsymbol{b}$, given by

1) $\mathbf{A}\boldsymbol{x} = \boldsymbol{b}$ has only one solution, if $\mathrm{rank}\left(\begin{bmatrix}\mathbf{A} & \boldsymbol{b}\end{bmatrix}\right) = \mathrm{rank}(\mathbf{A}) = c$;
2) $\mathbf{A}\boldsymbol{x} = \boldsymbol{b}$ has infinite solutions, if $\mathrm{rank}\left(\begin{bmatrix}\mathbf{A} & \boldsymbol{b}\end{bmatrix}\right) = \mathrm{rank}(\mathbf{A}) < c$;
3) $\mathbf{A}\boldsymbol{x} = \boldsymbol{b}$ has no solution, if $\mathrm{rank}(\mathbf{A}) < \mathrm{rank}\left(\begin{bmatrix}\mathbf{A} & \boldsymbol{b}\end{bmatrix}\right)$.

[1]For a matrix $\mathbf{F} \in \mathbb{R}^{m\times n}$, the Moore-Penrose inverse of $\mathbf{F}$ is defined as $\mathbf{F}^+ \in \mathbb{R}^{n\times m}$. Moreover, if $\mathrm{rank}(\mathbf{F}) = m$, it has $\mathbf{F}\mathbf{F}^+ = \mathbf{I}_m$. If $\mathrm{rank}(\mathbf{F}^{\mathrm{T}}) = n$, it has and $\mathbf{F}^+\mathbf{F} = \mathbf{I}_n$. [41]

D. Nonsmooth Analysis [45]

Consider the following differential equation:

$$\dot{\boldsymbol{x}}(t) = \mathfrak{f}\,(t, \boldsymbol{x}(t))\,, \qquad \boldsymbol{x}(0) = \boldsymbol{x}_0, \qquad t > 0, \tag{2}$$

where $\mathfrak{f} : \mathbb{R} \times \mathbb{R}^q \to \mathbb{R}^q$ is measurable and essentially locally bounded. Let $\mathcal{F}\left[\mathfrak{f}\,(t, \boldsymbol{x}(t))\right]$ denote the *Filippov set-valued map*, such that

$$\mathcal{F}\left[\mathfrak{f}\,(t, \boldsymbol{x}(t))\right] \triangleq \bigcap_{\delta>0} \bigcap_{u(\boldsymbol{\mathcal{S}})=0} \overline{\mathrm{co}}\left\{\mathfrak{f}\,(t, \boldsymbol{\mathcal{B}}_\delta\,(\boldsymbol{x}) \setminus \boldsymbol{\mathcal{S}})\right\},$$

where $\bigcap_{u(\boldsymbol{\mathcal{S}})=0}$ denotes the intersection over all sets $\boldsymbol{\mathcal{S}}$ of Lebesgue measure zero; $\overline{\mathrm{co}}$ denotes the convex closure.

The *Filippov solution* of (2) is defined by an absolutely continuous vector function $\boldsymbol{x} \in \mathbb{R}^q$ on $[0, \tau]$, such that

$$\dot{\boldsymbol{x}}(t) \in \mathcal{F}\left[\mathfrak{f}\,(t, \boldsymbol{x}(t))\right] \quad \text{for almost all} \quad t \in [0, \tau]\,.$$

For a locally Lipschitz function $W(\boldsymbol{x}(t))$: $\mathbb{R}^q \to \mathbb{R}$, the *generalized gradient* of $W(\boldsymbol{x}(t))$ at $\boldsymbol{x}(t)$ is defined as

$$\partial W(\boldsymbol{x}) \triangleq \mathtt{co}\left\{\lim_{\boldsymbol{w}\to\boldsymbol{x}} \nabla W(\boldsymbol{x}) : \boldsymbol{w} \notin \boldsymbol{\Omega}_w \cup \boldsymbol{\mathcal{S}}\right\},$$

where $\mathtt{co}$ denotes the convex hull; $\boldsymbol{\Omega}_w$ is the set of points in which $W(\boldsymbol{x}(t))$ is not differentiable; $\boldsymbol{\mathcal{S}}$ is a set of measure zero that can be arbitrarily chosen so as to simplify the calculation. The *set-valued Lie derivative* of $W(\boldsymbol{x}(t))$ with respect to (2) at $\boldsymbol{x}(t)$ is defined by

$$\mathcal{L}_{\mathrm{Eq.(2)}} W(\boldsymbol{x}) \triangleq \bigcap_{\boldsymbol{\xi}\in\partial W(\boldsymbol{x})} \boldsymbol{\xi}^{\mathrm{T}} \mathcal{F}\left[\mathfrak{f}\right].$$

E. Some Useful Lemmas

Lemma 1 ([46]): For the system $\dot{\boldsymbol{x}} = \boldsymbol{f}\,(t, \boldsymbol{x})$, if there exists a $\mathcal{C}^1$ function $V\,(\boldsymbol{x}) \geq 0$, such that $\dot{V}\,(\boldsymbol{x}) \leq -k_1 V\,(\boldsymbol{x}) - k_2 V\,(\boldsymbol{x})^q$, where $k_1 > 0$, $k_2 > 0$, and $0 < q < 1$, then the closed-loop system is finite-time stable, and the settling time is calculated by

$$T = \frac{1}{k_1\,(1-q)} \ln \frac{k_1 V^{1-q}\,(\boldsymbol{x}(0)) - k_2}{k_2}.$$

Lemma 2 ([47]): For the system $\dot{\boldsymbol{x}} = \boldsymbol{f}\,(t, \boldsymbol{x})$, if there exists a $\mathcal{C}^1$ function $V\,(\boldsymbol{x}) \geq 0$, such that $\dot{V}\,(\boldsymbol{x}) \leq -k_3 V\,(\boldsymbol{x})^q$, where $k_3 > 0$, and $0 < q < 1$, then the closed-loop system is finite-time stable, and the settling time is calculated by

$$T = \frac{V^{1-q}\,(\boldsymbol{x}(0))}{k_3\,(1-q)}.$$

Lemma 3 (Corollary 24 of [48]): Consider the cascade-connected system

$$\begin{cases} \dot{\boldsymbol{x}}_1 = \boldsymbol{f}_1\,(t, \boldsymbol{x}_1, \boldsymbol{x}_2) \\ \dot{\boldsymbol{x}}_2 = \boldsymbol{f}_2\,(t, \boldsymbol{x}_2) \end{cases}, \tag{3}$$

where $\boldsymbol{f}_1 : \mathbb{R} \times \mathbb{R}^{n_1} \times \mathbb{R}^{n_2} \to \mathbb{R}^{n_1}$ and $\boldsymbol{f}_2 : \mathbb{R} \times \mathbb{R}^{n_2} \to \mathbb{R}^{n_2}$ are Lipschitz continuous. $\boldsymbol{f}_1\,(\cdot, \boldsymbol{0}_{n_1}, \boldsymbol{0}_{n_2}) \equiv \boldsymbol{0}_{n_1}$, $\boldsymbol{f}_2\,(\cdot, \boldsymbol{0}_{n_2}) \equiv \boldsymbol{0}_{n_2}$. Then the equilibrium $(\boldsymbol{x}_1, \boldsymbol{x}_2) = (\boldsymbol{0}_{n_1}, \boldsymbol{0}_{n_2})$ is uniformly globally asymptotically stable[2] (UGAS) for (3) if and only if the following three conditions are satisfied:

[2]A system is UGAS if it is uniformly globally stable, and uniformly globally attractive [48], [49].

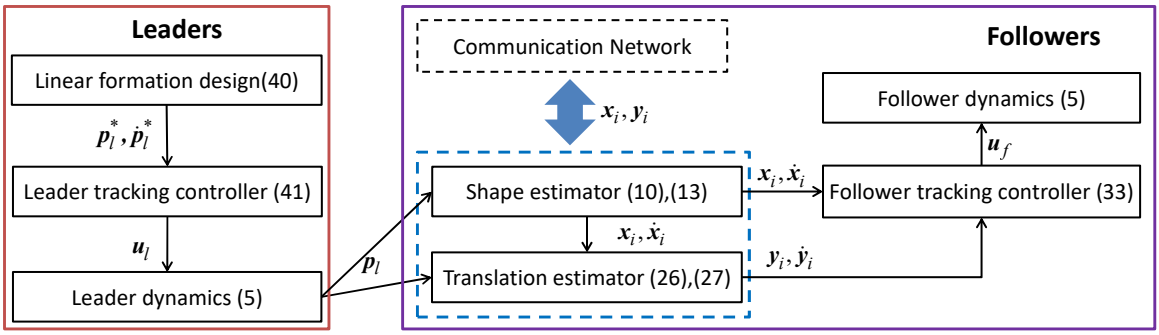

Fig. 1. Information flow of the proposed estimation-based time-varying linear formation control schemes. $\boldsymbol{u_l}$, and $\boldsymbol{u_f}$ denotes the control inputs of all leaders and followers, respectively.

1) The equilibrium $\boldsymbol{x}_1 = \boldsymbol{0}_{n_1}$ is UGAS for $\dot{\boldsymbol{x}}_1 = \boldsymbol{f}_1(t, \boldsymbol{x}_1, \boldsymbol{0}_{n_2})$.
2) The equilibrium $\boldsymbol{x}_2 = \boldsymbol{0}_{n_2}$ is UGAS for $\dot{\boldsymbol{x}}_2 = \boldsymbol{f}_1(t, \boldsymbol{x}_2)$.
3) All solutions of (3) are t_0-*uniformly bounded*[3], i.e., $\mathbb{BS} = \mathbb{R}^{n_1} \times \mathbb{R}^{n_2}$.

III. Problem Statement

A. Time-varying Linear Formation Control Architecture

First, we introduce some definitions in the time-varying linear formation control architecture to describe desired formations during maneuvers.

Definition 1 (Nominal configuration): The nominal configuration $\{\boldsymbol{r}_i(t)\}_{i=1}^n$, $\boldsymbol{r}_i(t) \in \mathbb{R}^f$ is a set of pre-defined time-varying vectors corresponding to each agent.

Definition 2 (Augmented nominal configuration): $\bar{\boldsymbol{r}}_i(t) = \begin{bmatrix} \boldsymbol{r}_i^{\mathrm{T}}(t) & 1 \end{bmatrix}^{\mathrm{T}} \in \mathbb{R}^{f+1}$ is called the augmented nominal configuration.

Definition 3 (Target formation): The target formation $\boldsymbol{p}_i^*(t) \in \mathbb{R}^d$ is the desired position of agent i, with $d \leq f$. It is a linear transformation of the augmented nominal configuration, i.e.,

$$\boldsymbol{p}_i^*(t) = \bar{\mathbf{A}}(t)\bar{\boldsymbol{r}}_i(t) = \mathbf{A}(t)\boldsymbol{r}_i(t) + \boldsymbol{b}(t), \tag{4}$$

where $\mathbf{A}(t) \in \mathbb{R}^{d\times f}$ is the linear transformation matrix; $\boldsymbol{b}(t) \in \mathbb{R}^d$; $\bar{\mathbf{A}}(t) = \begin{bmatrix} \mathbf{A}(t) & \boldsymbol{b}(t) \end{bmatrix} \in \mathbb{R}^{d\times(f+1)}$. $\mathbf{A}(t)\boldsymbol{r}_i(t)$ and $\boldsymbol{b}(t)$ represent the shape and translation of formation, respectively. All possible target formations constitute the following set $\mathcal{T}(\bar{\boldsymbol{r}}(t))$, which exactly is the image space of the linear transformation $\bar{\mathbf{A}}(t)$, i.e.,

$$\mathcal{T}(\bar{\boldsymbol{r}}(t)) = \left\{\boldsymbol{p}^*(t) \in \mathbb{R}^{dn} : \boldsymbol{p}^*(t) = (\mathbf{I}_n \otimes \bar{\mathbf{A}}(t))\bar{\boldsymbol{r}}(t)\right\},$$

where

$$\boldsymbol{p}^*(t) = \left[(\boldsymbol{p}_1^*(t))^{\mathrm{T}} \quad \dots \quad (\boldsymbol{p}_n^*(t))^{\mathrm{T}}\right]^{\mathrm{T}},$$
$$\bar{\boldsymbol{r}}(t) = \left[\bar{\boldsymbol{r}}_1^{\mathrm{T}}(t) \quad \dots \quad \bar{\boldsymbol{r}}_n^{\mathrm{T}}(t)\right]^{\mathrm{T}}.$$

[3]Let $\boldsymbol{x}_0 \in \mathbb{R}^n$. The solutions with initial state $\boldsymbol{x}_0$ are t_0-uniformly bounded if there exist a const $c > 0$ such that $\boldsymbol{x}\left(\mathbb{R}_{\geq t_0}, t_0, \boldsymbol{x}_0\right) \subset \mathcal{B}_c(0)$ for all $t_0 \in \mathbb{R}$. The set of initial states giving rise to t_0-uniformly bounded solutions is defined as ([48])

$$\mathbb{BS} = \left\{\boldsymbol{x}_0 \in \mathbb{R}^n : (\exists c > 0)\,(\forall t_0 \in \mathbb{R})\,\boldsymbol{x}\left(\mathbb{R}_{\geq t_0}, t_0, \boldsymbol{x}_0\right) \subset \mathcal{B}_c(0)\right\}.$$

B. Problem Description

Consider a group of n agents in $\mathbb{R}^d$ and a time-varying nominal configuration in $\mathbb{R}^f$, where $d \in \mathbb{N}^+$ and $n \geq f+2$, $f \geq d$, $f \in \mathbb{N}^+$. The leader set $\mathcal{V}_l \subset \mathcal{V}$ consists n_l agents, and the remaining $n_f = n - n_l$ agents form the follower set $\mathcal{V}_f \subset \mathcal{V}$, where $\mathcal{V}$ denotes the set that comprises all agents.

Each agent satisfies the following single-integrator dynamics:

$$\dot{\boldsymbol{p}}_i(t) = \boldsymbol{u}_i(t), \qquad i = 1, ..., n, \tag{5}$$

where $\boldsymbol{u}_i(t) \in \mathbb{R}^d$ is control input, and $\boldsymbol{p}_i(t) \in \mathbb{R}^d$ represents the position.

The graph $\mathcal{G}$ denotes the communication topology among agents. This paper considers the first n_l agents are leaders without losing generality. The Laplacian matrix $\mathcal{L}$ associated with the graph $\mathcal{G}$ is defined in the following form according to the partition of leaders and followers:

$$\mathcal{L} = \begin{bmatrix} \mathcal{L}_{ll} & \mathcal{L}_{lf} \\ \mathcal{L}_{fl} & \mathcal{L}_{ff} \end{bmatrix}.$$

Let $\mathcal{G}_f$ denotes the subgraph of $\mathcal{G}$, consisting of all followers. The corresponding Laplacian matrix of $\mathcal{G}_f$ is represented by $\mathcal{L}_f$. $\mathcal{N}_i$ and $\mathcal{N}_{fi}$ denote the neighbor sets of the agent i in $\mathcal{G}$, and $\mathcal{G}_f$, respectively.

In this paper, only leaders know the time-varying augmented linear transformation matrix $\bar{\mathbf{A}}(t)$. Followers can communicate internally, but they cannot communicate with leaders. The only available information for followers is leaders' position measurements. Followers can estimate $\bar{\mathbf{A}}(t)$ using these measurements for achieving time-varying formation tracking. Let $\boldsymbol{x}_i(t)$ and $\boldsymbol{y}_i(t)$ denote the estimations of the formation shape $\boldsymbol{x}^*(t) = \mathrm{vec}(\mathbf{A}(t))$ and translation $\boldsymbol{y}^*(t) = \boldsymbol{b}(t)$, respectively. The primary objective of this study is to develop followers' cooperative estimation laws to obtain the precise $\boldsymbol{x}^*(t)$ and $\boldsymbol{y}^*(t)$ for achieving time-varying target formation tracking, i.e.,

$$\lim_{t\to\infty}\left[\boldsymbol{x}_i(t) - \boldsymbol{x}^*(t)\right] = \boldsymbol{0}_{df}, \tag{6}$$
$$\lim_{t\to\infty}\left[\boldsymbol{y}_i(t) - \boldsymbol{y}^*(t)\right] = \boldsymbol{0}_d, \tag{7}$$
$$\lim_{t\to\infty}\left[\boldsymbol{p}_i(t) - \bar{\mathbf{A}}(t)\bar{\boldsymbol{r}}_i(t)\right] = \boldsymbol{0}_d, \tag{8}$$

for $\forall i \in \mathcal{V}_f$, where $\bar{\mathbf{A}}(t)\bar{\boldsymbol{r}}_i(t) = \left(\boldsymbol{r}_i^{\mathrm{T}}(t) \otimes \mathbf{I}_d\right)\boldsymbol{x}^*(t) + \boldsymbol{y}^*(t)$.

In the following sections, we will achieve these three goals (6)-(8) in turn. For distributed algorithms, it is necessary to

assume that the graph is connected, so we make the following assumption.

Assumption 1: The subgraph $\mathcal{G}_f$ is undirected and connected.

Fig. 1 shows the proposed comprehensive set of time-varying linear formation control schemes. A linear formation planning method is given in Appendix A to generate $\boldsymbol{x}^*(t)$, $\boldsymbol{y}^*(t)$, and leaders' desired trajectories. For followers, their shape estimator, translation estimator, and tracking controller will be explained in detail in Section IV, V, and VI, respectively. Since the designed trajectories of leaders can be informed to leaders, we also make the following assumption for leaders.

Assumption 2: Leaders are equipped with appropriate feedback controllers that can let leaders track their desired trajectories, i.e.,

$$\lim_{t\to\infty}\tilde{\boldsymbol{p}}_i(t)=\boldsymbol{0}_d,\qquad \forall i\in\boldsymbol{\mathcal{V}}_l.$$

where the leader's position error is defined as $\tilde{\boldsymbol{p}}_i(t)\triangleq\boldsymbol{p}_i(t)-\boldsymbol{p}_i^*(t)$, $\forall i\in\boldsymbol{\mathcal{V}}_l$.

C. Uniqueness of Target Formation

Since the proposed time-varying linear formation control architecture has a leader-follower structure, it is necessary to ensure that leaders can uniquely determine the target formation. Therefore, the concept of "linear localizability" is introduced here.

Definition 4 (Linear localizability): For the nominal configuration $\{\boldsymbol{r}_i(t)\}_{i=1}^n$ of n agents, if any feasible $\boldsymbol{p}_f^*(t)$ can be uniquely determined by $\boldsymbol{p}_l^*(t)$, the nominal configuration $\{\boldsymbol{r}_i(t)\}_{i=1}^n$ is said to be linearly localizable, where $\boldsymbol{p}_l^*(t)$ and $\boldsymbol{p}_f^*(t)$ denote the target formations (determined by (4)) of leaders and followers, respectively.

$$\boldsymbol{p}_l^*(t)=\begin{bmatrix}(\boldsymbol{p}_1^*(t))^{\mathrm{T}} & \dots & (\boldsymbol{p}_{n_l}^*(t))^{\mathrm{T}}\end{bmatrix}^{\mathrm{T}},$$
$$\boldsymbol{p}_f^*(t)=\begin{bmatrix}(\boldsymbol{p}_{n_l+1}^*(t))^{\mathrm{T}} & \dots & (\boldsymbol{p}_n^*(t))^{\mathrm{T}}\end{bmatrix}^{\mathrm{T}}.$$

Remark 1: If the nominal formation lies in the same Euclidean space as that of agents' coordinates (i.e., $f=d$), the concept of linear localizability is the same as the affine localizability introduced in [14]. However, high-dimensional nominal formations are allowed in linear localizability, which implies linear localizability is more general in terms of formation representations.

This section shows that linear localizability for a nominal configuration can be guaranteed by the following assumption.

Assumption 3: For the time-varying nominal configuration $\{\boldsymbol{r}_i(t)\}_{i=1}^n$, $\boldsymbol{r}_i(t)\in\mathbb{R}^f$, it is assumed that $\{\boldsymbol{r}_i(t)\}_{i\in\boldsymbol{\mathcal{V}}_l}$ linearly span $\mathbb{R}^f$, i.e,

$$\text{span}\{\boldsymbol{r}_1(t),...,\boldsymbol{r}_{n_l}(t)\}=\mathbb{R}^f.$$

A necessary condition for Assumption 3 is $n_l\geq f+1$, which implies that the minimum number of leaders is $f+1$.

Remark 2: In order to generate time-varying $\{\boldsymbol{r}_i(t)\}_{i=1}^n$ that satisfies Assumption 3. For a $\{\boldsymbol{r}_i(0)\}_{i=1}^n$ that meets Assumption 3, one can let the member of $\{\boldsymbol{r}_i(t)\}_{i=1}^n$ move alone its corresponding linear sub-spaces, i.e., periodically scaling as we selected in the simulation (Section VII-A). Alternatively, it is also tenable to maintain linear spatial complementary relations among $\{\boldsymbol{r}_i(0)\}_{i=1}^n$ by multiplying the same time-varying f-dimensional rotation matrix.

To begin, we introduce a lemma adapted from the affine formation control [13], [14].

Lemma 4: For the nominal configuration $\{\boldsymbol{r}_i(t)\}_{i=1}^n$, $\boldsymbol{r}_i\in\mathbb{R}^f$, the following conditions 1)-3) are equivalent.

1) $\{\boldsymbol{r}_i(t)\}_{i=1}^n$ linearly span $\mathbb{R}^f$.
2) $\text{rank}(\bar{\mathbf{R}}(t))=f+1$, where

$$\bar{\mathbf{R}}(t)=\begin{bmatrix}\bar{\mathbf{R}}_l^{\mathrm{T}}(t) & \bar{\mathbf{R}}_f^{\mathrm{T}}(t)\end{bmatrix}^{\mathrm{T}}\in\mathbb{R}^{n\times(f+1)},$$
$$\bar{\mathbf{R}}_l(t)=\begin{bmatrix}\bar{\boldsymbol{r}}_1(t) & \dots & \bar{\boldsymbol{r}}_{n_l}(t)\end{bmatrix}^{\mathrm{T}}\in\mathbb{R}^{n_l\times(f+1)},$$
$$\bar{\mathbf{R}}_f(t)=\begin{bmatrix}\bar{\boldsymbol{r}}_{n_l+1}(t) & \dots & \bar{\boldsymbol{r}}_n(t)\end{bmatrix}^{\mathrm{T}}\in\mathbb{R}^{(n-n_l)\times(f+1)}.$$

3) $\dim(\mathcal{T}(\bar{\boldsymbol{r}}(t)))=(f+1)d$.

Proof: See Lemma 2 of [50]. □

Now, we introduce the following theorem to formally give the necessary and sufficient conditions for linear localizability.

Theorem 1: The time-varying nominal configuration $\{\boldsymbol{r}_i(t)\}_{i=1}^n$, $\boldsymbol{r}_i(t)\in\mathbb{R}^f$ is linearly localizable, if and only if $\{\boldsymbol{r}_i(t)\}_{i=1}^n$ satisfies Assumption 3. Further,

$$\boldsymbol{p}_f^*(t)=(\bar{\mathbf{R}}_f(t)\otimes\mathbf{I}_d)(\bar{\mathbf{R}}_l^+(t)\otimes\mathbf{I}_d)\boldsymbol{p}_l^*(t).$$

Proof: In this proof, we will omit argument t when it is clear that we are referring to $\boldsymbol{r}_i(t)$, $\boldsymbol{p}_l^*(t)$, $\boldsymbol{p}_f^*(t)$, $\bar{\mathbf{R}}_l(t)$, $\bar{\mathbf{R}}_f(t)$, and $\bar{\mathbf{A}}(t)$.

(Sufficiency) Note that $\boldsymbol{p}_l^*$ is determined by the linear transformation $\bar{\mathbf{A}}$, such that

$$\boldsymbol{p}_l^*=\left(\mathbf{I}_{n_l}\otimes\bar{\mathbf{A}}\right)\bar{\boldsymbol{r}}_l=(\bar{\mathbf{R}}_l\otimes\mathbf{I}_d)\text{vec}(\bar{\mathbf{A}}).\tag{9}$$

where $\boldsymbol{r}_l=\begin{bmatrix}\boldsymbol{r}_1^{\mathrm{T}} & \dots & \boldsymbol{r}_{n_l}^{\mathrm{T}}\end{bmatrix}^{\mathrm{T}}$. If $\{\boldsymbol{r}_i(t)\}_{i\in\boldsymbol{\mathcal{V}}_l}$ linearly span $\mathbb{R}^f$, according to Lemma 4, it can be derived that $\text{rank}(\bar{\mathbf{R}}_l)=f+1$ and $n_l\geq f+1$. Then, $\text{vec}(\bar{\mathbf{A}})$ can be uniquely obtained by

$$\text{vec}(\bar{\mathbf{A}})=(\bar{\mathbf{R}}_l^+\otimes\mathbf{I}_d)\boldsymbol{p}_l^*.$$

Then, by using the above equality, followers' target positions are uniquely computed by

$$\begin{aligned}\boldsymbol{p}_f^*=\left(\mathbf{I}_{n_f}\otimes\bar{\mathbf{A}}\right)\bar{\boldsymbol{r}}_f&=(\bar{\mathbf{R}}_f\otimes\mathbf{I}_d)\text{vec}(\bar{\mathbf{A}})\\&=(\bar{\mathbf{R}}_f\otimes\mathbf{I}_d)(\bar{\mathbf{R}}_l^+\otimes\mathbf{I}_d)\boldsymbol{p}_l^*,\end{aligned}$$

where $\bar{\boldsymbol{r}}_f=\begin{bmatrix}\bar{\boldsymbol{r}}_{n_l+1}^{\mathrm{T}} & \dots & \bar{\boldsymbol{r}}_n^{\mathrm{T}}\end{bmatrix}^{\mathrm{T}}$. The linear localizability is proven.

(Necessity) If $\{\boldsymbol{r}_i\}_{i\in\boldsymbol{\mathcal{V}}_l}$ do not linearly span $\mathbb{R}^f$, it means $\text{rank}(\bar{\mathbf{R}}_l)<f+1$. Then, in view of Section II-C, we know that $\text{rank}(\bar{\mathbf{R}}_l)<f+1$ does not satisfy the rank conditions for the system of linear equations (9) having the unique solution about $\text{vec}(\bar{\mathbf{A}})$. Hence, $\text{vec}(\bar{\mathbf{A}})$ can not be located, nor does $\boldsymbol{p}_f^*$. ■

IV. Cooperative Linear Formation Shape Estimator Design

This section describes a distributed method for followers to cooperatively estimate the formation shape $\boldsymbol{x}^*(t)$. This estimation is achieved through measuring relative displacements of leaders. The displacement measurability is defined as follows.

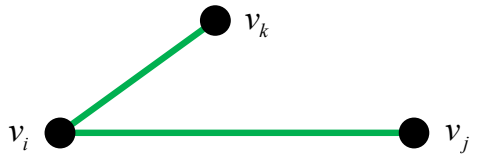

Fig. 2. The subgraph corresponding to the triplet $\tau_{ji,ki}$.

Definition 5 (Displacement measurability): In the graph $\mathcal{G}$, if there exists a triplet[4] $\tau_{ji,ki}$, we say the displacement corresponding to the edge (v_j, v_k) is measurable by agent i.

Consider n_{f1} followers are capable of measuring leaders' edges, forming the set $\mathcal{V}_{f1}$. The remaining n_{f2} followers constitute the set $\mathcal{V}_{f2}$. It satisfies $\mathcal{V}_f = \mathcal{V}_{f1} \cup \mathcal{V}_{f2}$, $\mathcal{V}_{f1} \cap \mathcal{V}_{f2} = \varnothing$, $n_{f1} + n_{f2} = n_f$, $n_{f1} \in \mathbb{N}^+$, $n_{f2} \in \mathbb{N}$. Without losing generality, this paper considers that the first n_{f1} followers can measure leaders' edges.

Let $\boldsymbol{x}_i(t) \in \mathbb{R}^{df}$ represent the local estimation of $\boldsymbol{x}^*(t)$ for follower i. This local estimation satisfies the following integrator dynamics:

$$\dot{\boldsymbol{x}}_i(t) = \boldsymbol{\mu}_i(t), \qquad i \in \mathcal{V}_f, \tag{10}$$

where $\boldsymbol{\mu}_i(t) \in \mathbb{R}^{df}$.

A. Observability Analysis

This subsection shows that the following Assumption 4 is the sufficient condition for ensuring that $\boldsymbol{x}^*(t)$ is available by followers.

Assumption 4: In the time-varying nominal configuration $\{\boldsymbol{r}_i(t)\}_{i=1}^n$, $\boldsymbol{r}_i(t) \in \mathbb{R}^f$, all leaders' measurable edge displacements linearly span $\mathbb{R}^f$, i.e.,

$$\text{span}\{..., \boldsymbol{r}_{jk}(t), ...\} = \mathbb{R}^f, \quad \text{for all } \mathcal{G}_s(\tau_{ji,ki}) \subset \mathcal{G},$$

where $i \in \mathcal{V}_{f1}$; $j, k \in \mathcal{V}_l$; $\boldsymbol{r}_{jk}(t) = \boldsymbol{r}_j(t) - \boldsymbol{r}_k(t)$.

It is noted that Assumption 3 is the necessary condition for Assumption 4. Let m_i denote the number of leaders' edge displacements that follower i can measure, where $i \in \mathcal{V}_{f1}$. These measurable m_i edge displacements establish the following time-varying linear sub-equation

$$\mathbf{M}_i(t)\boldsymbol{z}(t) = \boldsymbol{\xi}_i(t), \tag{11}$$

where $\mathbf{M}_i(t) \in \mathbb{R}^{dm_i \times df}$, $\boldsymbol{z}(t) \in \mathbb{R}^{df}$, $\boldsymbol{\xi}_i(t) \in \mathbb{R}^{m_i}$,

$$\begin{aligned}
\mathbf{M}_i(t) &= \begin{bmatrix} \cdots & \left(\boldsymbol{r}_{jk}^{\mathrm{T}}(t) \otimes \mathbf{I}_d\right)^{\mathrm{T}} & \cdots \end{bmatrix}^{\mathrm{T}}, \quad j,k \in \mathcal{V}_l \cap \mathcal{N}_i, \\
\boldsymbol{\xi}_i(t) &= \begin{bmatrix} \cdots & \boldsymbol{p}_{jk}^{\mathrm{T}}(t) & \cdots \end{bmatrix}^{\mathrm{T}}, \qquad\qquad j,k \in \mathcal{V}_l \cap \mathcal{N}_i, \\
\boldsymbol{p}_{jk}(t) &= \boldsymbol{p}_j(t) - \boldsymbol{p}_k(t).
\end{aligned}$$

According to the size of $\mathbf{M}_i(t)$, it is noticed that dm_i may be smaller than df. Then, in view of Section II-C, $\boldsymbol{z}(t)$ may not be unique determined by (11), i.e., $\boldsymbol{x}^*(t)$ is only one element of the solution of (11). This observation implies that the target formation shape $\boldsymbol{x}^*(t)$ typically cannot be located by the measurements from a single follower i through (11).

All followers in $\mathcal{V}_{f1}$ admit the following time-varying linear equation

$$\mathbf{M}(t)\boldsymbol{z}(t) = \boldsymbol{\xi}(t), \tag{12}$$

where $\mathbf{M}(t) \in \mathbb{R}^{m \times df}$; $\boldsymbol{\xi}(t) \in \mathbb{R}^m$; $\sum_{i \in \mathcal{V}_{f1}} m_i = m$. It follows

$$\mathbf{M}(t) = \begin{bmatrix} \mathbf{M}_{n_l+1}(t) \\ \vdots \\ \mathbf{M}_{n_l+n_{f1}}(t) \end{bmatrix}, \quad \boldsymbol{\xi}(t) = \begin{bmatrix} \boldsymbol{\xi}_{n_l+1}(t) \\ \vdots \\ \boldsymbol{\xi}_{n_l+n_{f1}}(t) \end{bmatrix}.$$

If Assumption 4 is satisfied, it has $\text{rank}(\mathbf{M}(t)) = df$. In view of Section II-C, Eq.(12) must have a unique or no solution. Since all leaders' positions are governed by the same formation shape parameter $\boldsymbol{x}^*(t)$, there must exist the solution of (12). Therefore, it is concluded that (12) has the unique solution $\boldsymbol{x}^*(t)$, i.e., $\boldsymbol{z}(t) = \boldsymbol{x}^*(t)$.

B. Estimator Design

Based on the analysis in the previous subsection, it is observed that the cooperative estimation of $\boldsymbol{x}^*(t)$ essentially involves solving the system of time-varying linear equations (12) in a distributed manner. To facilitate it, we make two assumptions about the boundness of the following variables:

Assumption 5: The derivative of $\boldsymbol{x}^*(t)$ is bounded by $||\dot{\boldsymbol{x}}^*(t)||_2 < \delta_1$, where $\delta_1 > 0$.

Assumption 6: The leaders' velocity is bounded by $||\dot{\boldsymbol{p}}_i(t)||_2 < \delta_2$, $\forall i \in \mathcal{V}_l$, where $\delta_2 > 0$.

Let $\mathcal{M}_i(t) \triangleq \{\boldsymbol{z}(t) \in \mathbb{R}^n : \mathbf{M}_i(t)\boldsymbol{z}(t) = \boldsymbol{\xi}_i(t)\}$ represent the time-varying manifold corresponding to the linear sub-equation (11). Two sub-objectives for local estimations $\{\boldsymbol{x}_i(t)\}_{i \in \mathcal{V}_f}$ are given as follows:

1) For each follower belonging to $\mathcal{V}_{f1}$, the local estimation $\boldsymbol{x}_i(t)$ converge to its time-varying manifold $\mathcal{M}_i(t)$.
2) For all followers, their local estimations $\{\boldsymbol{x}_i(t)\}_{i \in \mathcal{V}_f}$ reach consensus.

The first sub-objective ensures that each local estimation of the follower belonging to $\mathcal{V}_{f1}$ satisfies its corresponding time-varying local linear sub-equation (11). The second sub-objective ensures that all followers admit the same local solution to the system of linear equations (12). If local estimations $\{\boldsymbol{x}_i(t)\}_{i \in \mathcal{V}_f}$ fulfill the above two sub-objectives simultaneously, it concludes that every local estimation is the solution of (12). To achieve those two sub-objectives, we propose the following distributed algorithm to solve (12) and obtain $\boldsymbol{x}^*(t)$ cooperatively.

$$\boldsymbol{\mu}_i(t) = \begin{cases} \boldsymbol{g}_i(t) + \boldsymbol{f}_i(t) & i \in \mathcal{V}_{f1} \\ \boldsymbol{g}_i(t) & i \in \mathcal{V}_{f2} \end{cases}, \tag{13}$$

$$\begin{aligned}
\boldsymbol{f}_i(t) = &- [\alpha + \beta_i(t)]\, \mathbf{M}_i^{\mathrm{T}}(t) \left[\mathbf{M}_i(t)\mathbf{M}_i^{\mathrm{T}}(t)\right]^{-1} [\mathbf{M}_i(t)\boldsymbol{x}_i(t) - \boldsymbol{\xi}_i(t)] \\
&- \gamma_i \mathbf{M}_i^{\mathrm{T}}(t) \left[\mathbf{M}_i\mathbf{M}_i^{\mathrm{T}}(t)\right]^{-1} \text{sgn}\,[\mathbf{M}_i(t)\boldsymbol{x}_i(t) - \boldsymbol{\xi}_i(t)] \\
&- \mathbf{M}_i^{\mathrm{T}}(t) \left[\mathbf{M}_i(t)\mathbf{M}_i^{\mathrm{T}}(t)\right]^{-1} \dot{\mathbf{M}}_i(t)\boldsymbol{x}_i(t),
\end{aligned} \tag{14}$$

[4]The triplet $\tau_{ji,ki}$ admits a subgraph $\mathcal{G}_s(\tau_{ji,ki})$ consisting of three nodes and two edges, such that $\mathcal{G}_s(\tau_{ji,ki}) = (\mathcal{V}_s(\tau_{ji,ki}), \mathcal{E}_s(\tau_{ji,ki})) \subseteq \mathcal{G}$, where $\mathcal{V}_s(\tau_{ji,ki}) = \{v_i, v_j, v_k\}$, $\mathcal{E}_s(\tau_{ji,ki}) = \{(v_j, v_i), (v_k, v_i)\}$. Please refer to Fig. 2.

$$\boldsymbol{g}_i(t) = -k\boldsymbol{\Pi}_i(t)\mathrm{sgn}\left[\boldsymbol{\Pi}_i(t)\sum_{j\in\mathcal{N}_i^f}(\boldsymbol{x}_i(t)-\boldsymbol{x}_j(t))\right], \quad (15)$$

where

$$\boldsymbol{\Pi}_i(t) = \begin{cases}\mathbf{P}_i(t) & i\in\boldsymbol{\mathcal{V}}_{f1}\\ \mathbf{I}_{df} & i\in\boldsymbol{\mathcal{V}}_{f2}\end{cases},$$
$$\beta_i(t) = \begin{cases}\left\|\dot{\mathbf{P}}_i(t)\right\|_\infty & i\in\boldsymbol{\mathcal{V}}_{f1}\\ 0 & i\in\boldsymbol{\mathcal{V}}_{f2}\end{cases},$$

$\alpha>0$, $\gamma_i>2m_i\delta_2$, and $k>\delta_1$. $\mathbf{P}_i(t)\in\mathbb{R}^{df\times df}$ denotes the orthogonal projection matrix, i.e.,

$$\mathbf{P}_i(t) = \mathbf{I}_{df} - \mathbf{M}_i^{\mathrm{T}}(t)\left[\mathbf{M}_i(t)\mathbf{M}_i^{\mathrm{T}}(t)\right]^{-1}\mathbf{M}_i(t).$$

If we consider a non-zero vector $\boldsymbol{v}\in\mathbb{R}^n$, its projection onto the tangent space of the manifold $\boldsymbol{\mathcal{M}}_i(t)$ is denoted by $\mathbf{P}_i(t)\boldsymbol{v}$.

In (13), terms $\boldsymbol{f}_i(t)$ and $\boldsymbol{g}_i(t)$ are designed to make local estimations converge to time-varying manifolds $\{\boldsymbol{\mathcal{M}}_i(t)\}_{i\in\boldsymbol{\mathcal{V}}_{f1}}$ and reach consensus, respectively. Now, we state the following theorems.

Theorem 2: Under Assumptions 2 and 6, for followers belonging to $\boldsymbol{\mathcal{V}}_{f1}$, the distributed algorithm (13) can let the local estimation $\boldsymbol{x}_i(t)$ with dynamics (10) to converge to the time-varying manifold $\boldsymbol{\mathcal{M}}_i(t)$ in finite time T_i, i.e.,

$$\lim_{t\to T_i}\left[\mathbf{M}_i(t)\boldsymbol{x}_i(t)-\boldsymbol{\xi}_i(t)\right] = \boldsymbol{0}_{dm_i}, \qquad \forall i\in\boldsymbol{\mathcal{V}}_{f1},$$

where

$$T_i = \frac{1}{2\left(\gamma_i-2m_i\delta_2\right)}\ln\frac{\left(\gamma_i-2m_i\delta_2\right)V_{i\varepsilon}^{\frac{1}{2}}(0)-2\alpha}{2\alpha},$$
$$V_{i\varepsilon}(t) = \frac{1}{2}\boldsymbol{\varepsilon}_i^{\mathrm{T}}(t)\boldsymbol{\varepsilon}_i(t),$$
$$\boldsymbol{\varepsilon}_i(t) = \mathbf{M}_i(t)\boldsymbol{x}_i(t)-\boldsymbol{\xi}_i(t).$$

Proof: The proof will be accomplished by analyzing the convergence of $\boldsymbol{\varepsilon}_i(t)$, which represents the convergence error to the time-varying manifold $\boldsymbol{\mathcal{M}}_i(t)$. The dynamics of $\boldsymbol{\varepsilon}_i(t)$ is given by

$$\dot{\boldsymbol{\varepsilon}}(t) = \dot{\mathbf{M}}_i(t)\boldsymbol{x}_i(t)+\mathbf{M}_i(t)\boldsymbol{\mu}_i(t)-\dot{\boldsymbol{\xi}}_i(t). \quad (16)$$

We consider a Lyapunov function candidate $V_{i\varepsilon}(t) = \frac{1}{2}\boldsymbol{\varepsilon}_i^{\mathrm{T}}(t)\boldsymbol{\varepsilon}_i(t)$, whose set-valued Lie derivative with respect to (16) is obtained by

$$\mathcal{L}_{\mathrm{Eq.(16)}}V_{i\varepsilon}(t) = \boldsymbol{\varepsilon}_i^{\mathrm{T}}(t)\mathcal{F}\left\{\dot{\boldsymbol{\varepsilon}}_i(t)\right\}.$$

Note that $\boldsymbol{g}_i(t)$ lies in the null space of $\mathbf{M}_i$, i.e., $\mathbf{M}_i(t)\boldsymbol{g}_i(t)\equiv\boldsymbol{0}_{m_i}$. It gives

$$\mathcal{L}_{\mathrm{Eq.(16)}}V_{i\varepsilon}(t) = -\left(\alpha+\beta_i(t)\right)\left\|\boldsymbol{\varepsilon}_i(t)\right\|_2^2 - \boldsymbol{\varepsilon}_i^{\mathrm{T}}(t)\mathcal{F}\left\{\gamma_i\mathrm{sgn}\left(\boldsymbol{\varepsilon}_i(t)\right)+\dot{\boldsymbol{\xi}}_i(t)\right\}.$$

According to Assumption 6, it is also known that $\left\|\dot{\boldsymbol{\xi}}_i(t)\right\|_2 \le 2m_i\delta_2$. Therefore, for $\forall h\in -\boldsymbol{\varepsilon}_i^{\mathrm{T}}(t)\mathcal{F}\left\{\gamma_i\mathrm{sgn}\left(\boldsymbol{\varepsilon}_i(t)\right)+\dot{\boldsymbol{\xi}}_i(t)\right\}$, it has $h\le -\left(\gamma_i-2m_i\delta_2\right)\left\|\boldsymbol{\varepsilon}_i(t)\right\|_1$. In view of Section II-D, $\dot{V}_{i\varepsilon}(t)\in\mathcal{L}_{\mathrm{Eq.(16)}}V_{i\varepsilon}(t)$ for almost all $t\ge0$. It gives

$$\max\mathcal{L}_{\mathrm{Eq.(16)}}V_{i\varepsilon}(t) \le -2\alpha V_{i\varepsilon}(t) - 2\left(\gamma_i-2m_i\delta_2\right)V_{i\varepsilon}^{\frac{1}{2}}(t).$$

In view of Lemma 1, it follows $\boldsymbol{\varepsilon}_i(t)\to\boldsymbol{0}_{dm_i}$, $t\to T_i$, which implies that $\boldsymbol{x}_i(t)$ will converge to $\boldsymbol{\mathcal{M}}_i(t)$ in finite time, i.e., $\mathbf{M}_i(t)\boldsymbol{x}_i(t)\to\boldsymbol{\xi}_i(t)$, $t\to T_i$. ■

Before further analysis, we introduce the following lemma to conclude the positive definiteness of a matrix.

Lemma 5: Under Assumptions 1 and 4, the matrix $\left(\mathbf{I}_{df n_f}-\boldsymbol{\Pi}(t)\right)+\bar{\boldsymbol{\mathcal{L}}}_f$ is positive definite, where $\bar{\boldsymbol{\mathcal{L}}}_f = \boldsymbol{\mathcal{L}}_f\otimes\mathbf{I}_{df}$, $\boldsymbol{\Pi}(t) = \mathrm{diag}\left\{\boldsymbol{\Pi}_{n_l+1}(t),...,\boldsymbol{\Pi}_n(t)\right\}$.

Proof: See Appendix B. □

Now, based on Lemma 5, the consensus performance of local shape estimation $\boldsymbol{x}_i(t)$ is analyzed in the following theorem.

Theorem 3: Under Assumptions 1-6, for all followers, the local shape estimations $\{\boldsymbol{x}_i(t)\}_{i\in\boldsymbol{\mathcal{V}}_f}$ can reach consensus under the algorithm (13), i.e.,

$$\lim_{t\to\infty}\left[\boldsymbol{x}_i(t)-\boldsymbol{x}_j(t)\right] = \boldsymbol{0}_{df}, \qquad \forall i,j\in\boldsymbol{\mathcal{V}}_f.$$

Proof: In this proof, we will omit argument t when it is clear that we are referring to $\mathbf{M}_i(t)$, $\mathbf{P}_i(t)$, $\boldsymbol{\Pi}(t)$, β_i, $\boldsymbol{f}_i(t)$, $\boldsymbol{g}_i(t)$, $\boldsymbol{\mu}_i(t)$, $\boldsymbol{x}_i(t)$, $\boldsymbol{x}^*(t)$, and $\boldsymbol{\xi}_i(t)$.

The proof will be accomplished once the following steps are realized.

1) Derive the estimation error dynamics $\tilde{\boldsymbol{x}}_i$ form (13) and (10).
2) Simplify the estimation error dynamics $\tilde{\boldsymbol{x}}_i$ by using the result from Theorem 2.
3) A Lyapunov function candidate is considered to analyze the convergence of $\tilde{\boldsymbol{x}}_i$.

For step 1), the estimation error is defined as

$$\tilde{\boldsymbol{x}}_i \triangleq \boldsymbol{x}_i-\boldsymbol{x}^*.$$

We know that $\boldsymbol{x}^*$ also satisfies each local linear sub-equation, i.e., $\mathbf{M}_i\boldsymbol{x}^*=\boldsymbol{\xi}_i$. It follows that

$$\dot{\mathbf{M}}_i\boldsymbol{x}^*+\mathbf{M}_i\dot{\boldsymbol{x}}^* = \dot{\boldsymbol{\xi}}_i.$$

Based on the above equality of $\boldsymbol{x}^*$, let us use $\tilde{\boldsymbol{x}}_i$ to replace $\boldsymbol{x}_i$ in $\boldsymbol{f}_i$. It has

$$\begin{aligned}\boldsymbol{f}_i =& -\left(\alpha+\beta_i\right)\mathbf{M}_i^{\mathrm{T}}\left(\mathbf{M}_i\mathbf{M}_i^{\mathrm{T}}\right)^{-1}\left(\mathbf{M}_i\boldsymbol{x}_i-\mathbf{M}_i\boldsymbol{x}^*\right)\\ &-\gamma_i\mathbf{M}_i^{\mathrm{T}}\left(\mathbf{M}_i\mathbf{M}_i^{\mathrm{T}}\right)^{-1}\mathrm{sgn}\left(\mathbf{M}_i\boldsymbol{x}_i-\mathbf{M}_i\boldsymbol{x}^*\right)\\ &-\mathbf{M}_i^{\mathrm{T}}\left(\mathbf{M}_i\mathbf{M}_i^{\mathrm{T}}\right)^{-1}\dot{\mathbf{M}}_i\tilde{\boldsymbol{x}}_i-\mathbf{M}_i^{\mathrm{T}}\left(\mathbf{M}_i\mathbf{M}_i^{\mathrm{T}}\right)^{-1}\dot{\mathbf{M}}_i\boldsymbol{x}^*\\ =& -\left(\alpha+\beta_i\right)\left(\mathbf{I}_n-\mathbf{P}_i\right)\tilde{\boldsymbol{x}}_i\\ &-\gamma_i\mathbf{M}_i^{\mathrm{T}}\left(\mathbf{M}_i\mathbf{M}_i^{\mathrm{T}}\right)^{-1}\mathrm{sgn}\left(\mathbf{M}_i\tilde{\boldsymbol{x}}_i\right)\\ &-\mathbf{M}_i^{\mathrm{T}}\left(\mathbf{M}_i\mathbf{M}_i^{\mathrm{T}}\right)^{-1}\dot{\mathbf{M}}_i\tilde{\boldsymbol{x}}_i\\ &-\mathbf{M}_i^{\mathrm{T}}\left(\mathbf{M}_i\mathbf{M}_i^{\mathrm{T}}\right)^{-1}\left(\mathbf{M}_i\dot{\boldsymbol{x}}^*+\dot{\boldsymbol{\xi}}_i\right)\\ =& -\left(\alpha+\beta_i\right)\left(\mathbf{I}_n-\mathbf{P}_i\right)\tilde{\boldsymbol{x}}_i\\ &-\gamma_i\left(\mathbf{I}_n-\mathbf{P}_i\right)\mathbf{M}_i^{\mathrm{T}}\left(\mathbf{M}_i\mathbf{M}_i^{\mathrm{T}}\right)^{-1}\mathrm{sgn}\left(\mathbf{M}_i\tilde{\boldsymbol{x}}_i\right)\\ &-\left(\mathbf{I}_n-\mathbf{P}_i\right)\mathbf{M}_i^{\mathrm{T}}\left(\mathbf{M}_i\mathbf{M}_i^{\mathrm{T}}\right)^{-1}\dot{\mathbf{M}}_i\tilde{\boldsymbol{x}}_i\\ &+\left(\mathbf{I}_n-\mathbf{P}_i\right)\dot{\boldsymbol{x}}^*-\left(\mathbf{I}_n-\mathbf{P}_i\right)\mathbf{M}_i^{\mathrm{T}}\left(\mathbf{M}_i\mathbf{M}_i^{\mathrm{T}}\right)^{-1}\dot{\boldsymbol{\xi}}_i,\end{aligned}$$

where the following relation is used in the last equality:

$$\left(\mathbf{I}_n-\mathbf{P}_i\right)\mathbf{M}_i^{\mathrm{T}}\left(\mathbf{M}_i\mathbf{M}_i^{\mathrm{T}}\right)^{-1} = \mathbf{M}_i^{\mathrm{T}}\left(\mathbf{M}_i\mathbf{M}_i^{\mathrm{T}}\right)^{-1}.$$

Then, let us use $\tilde{\boldsymbol{x}}_i$ to replace $\boldsymbol{x}_i$ in $\boldsymbol{g}_i$. It has

$$\boldsymbol{g}_i = -k\boldsymbol{\Pi}_i \text{sgn}\left[\boldsymbol{\Pi}_i \sum_{j\in\mathcal{N}_i^f}(\tilde{\boldsymbol{x}}_i - \tilde{\boldsymbol{x}}_j)\right].$$

Now, for $i \in \boldsymbol{\mathcal{V}}_{f1}$, the dynamics of $\tilde{\boldsymbol{x}}_i$ is obtained by

$$\begin{aligned}\dot{\tilde{\boldsymbol{x}}}_i =&\dot{\boldsymbol{x}}_i - \dot{\boldsymbol{x}}^*\\ =&\boldsymbol{\mu}_i - \dot{\boldsymbol{x}}^*\\ =&-(\alpha+\beta_i)(\mathbf{I}_n - \boldsymbol{\Pi}_i)\tilde{\boldsymbol{x}}_i\\ &-(\mathbf{I}_n - \boldsymbol{\Pi}_i)\mathbf{M}_i^{\mathrm{T}}\left(\mathbf{M}_i\mathbf{M}_i^{\mathrm{T}}\right)^{-1}\dot{\mathbf{M}}_i\tilde{\boldsymbol{x}}_i\\ &-\gamma_i(\mathbf{I}_n - \boldsymbol{\Pi}_i)\mathbf{M}_i^{\mathrm{T}}\left(\mathbf{M}_i\mathbf{M}_i^{\mathrm{T}}\right)^{-1}\text{sgn}\left(\mathbf{M}_i\tilde{\boldsymbol{x}}_i\right)\\ &-(\mathbf{I}_n - \boldsymbol{\Pi}_i)\mathbf{M}_i^{\mathrm{T}}\left(\mathbf{M}_i\mathbf{M}_i^{\mathrm{T}}\right)^{-1}\dot{\boldsymbol{\xi}}_i\\ &-\boldsymbol{\Pi}_i\dot{\boldsymbol{x}}^* - k\boldsymbol{\Pi}_i\text{sgn}\left[\boldsymbol{\Pi}_i\sum_{j\in\mathcal{N}_i^f}(\tilde{\boldsymbol{x}}_i - \tilde{\boldsymbol{x}}_j)\right]\end{aligned} \tag{17}$$

For step 2), in view of Theorem 2, considering $i \in \boldsymbol{\mathcal{V}}_{f1}$ when $t > T_i$, it has

$$\mathbf{M}_i\boldsymbol{x}_i - \boldsymbol{\xi}_i = \boldsymbol{0}_{m_i}, \qquad \forall i \in \boldsymbol{\mathcal{V}}_{f1}. \tag{18}$$

According to (18) and the fact $\mathbf{M}_i\boldsymbol{x}^* = \boldsymbol{\xi}_i$, when $t > T_i$, it follows

$$\mathbf{M}_i\tilde{\boldsymbol{x}}_i = \boldsymbol{0}_{m_i}, \qquad \forall i \in \boldsymbol{\mathcal{V}}_{f1}. \tag{19}$$

Further, for any follower $i \in \boldsymbol{\mathcal{V}}_f$, it has

$$(\mathbf{I}_{df} - \boldsymbol{\Pi}_i)\tilde{\boldsymbol{x}}_i = \boldsymbol{0}_{m_i}, \tag{20}$$

which implies

$$\tilde{\boldsymbol{x}}_i = \boldsymbol{\Pi}_i\tilde{\boldsymbol{x}}_i. \tag{21}$$

We consider the derivative of (21). It follows

$$(\mathbf{I}_{df} - \boldsymbol{\Pi}_i)\dot{\tilde{\boldsymbol{x}}}_i = \dot{\boldsymbol{\Pi}}_i\tilde{\boldsymbol{x}}_i. \tag{22}$$

By using (19) and multiplying both sides of (17) by $(\mathbf{I}_{df} - \boldsymbol{\Pi}_i)$, it is obtained that

$$\begin{aligned}(\mathbf{I}_{df} - \boldsymbol{\Pi}_i)\dot{\tilde{\boldsymbol{x}}}_i =& -(\mathbf{I}_n - \mathbf{P}_i)\mathbf{M}_i^{\mathrm{T}}\left(\mathbf{M}_i\mathbf{M}_i^{\mathrm{T}}\right)^{-1}\dot{\mathbf{M}}_i\tilde{\boldsymbol{x}}_i\\ &-(\mathbf{I}_n - \mathbf{P}_i)\mathbf{M}_i^{\mathrm{T}}\left(\mathbf{M}_i\mathbf{M}_i^{\mathrm{T}}\right)^{-1}\dot{\boldsymbol{\xi}}_i.\end{aligned}$$

In view of the above equation and (22), we have

$$\begin{aligned}\dot{\boldsymbol{\Pi}}_i\tilde{\boldsymbol{x}}_i =& -(\mathbf{I}_{df} - \boldsymbol{\Pi}_i)\mathbf{M}_i^{\mathrm{T}}\left(\mathbf{M}_i\mathbf{M}_i^{\mathrm{T}}\right)^{-1}\dot{\mathbf{M}}_i\tilde{\boldsymbol{x}}_i\\ &-(\mathbf{I}_{df} - \boldsymbol{\Pi}_i)\mathbf{M}_i^{\mathrm{T}}\left(\mathbf{M}_i\mathbf{M}_i^{\mathrm{T}}\right)^{-1}\dot{\boldsymbol{\xi}}_i.\end{aligned}$$

Then, by multiplying both sides of the above equation by $(\mathbf{I}_{df} - \boldsymbol{\Pi}_i)$, it is obtained that

$$\begin{aligned}(\mathbf{I}_{df} - \boldsymbol{\Pi}_i)\dot{\boldsymbol{\Pi}}_i\tilde{\boldsymbol{x}}_i =& -(\mathbf{I}_{df} - \boldsymbol{\Pi}_i)\mathbf{M}_i^{\mathrm{T}}\left(\mathbf{M}_i\mathbf{M}_i^{\mathrm{T}}\right)^{-1}\dot{\mathbf{M}}_i\tilde{\boldsymbol{x}}_i\\ &-(\mathbf{I}_n - \boldsymbol{\Pi}_i)\mathbf{M}_i^{\mathrm{T}}\left(\mathbf{M}_i\mathbf{M}_i^{\mathrm{T}}\right)^{-1}\dot{\boldsymbol{\xi}}_i.\end{aligned} \tag{23}$$

Now, substituting (19) and (23) into (17), we obtain the error dynamics as following for $i \in \boldsymbol{\mathcal{V}}_{f1}$:

$$\begin{aligned}\dot{\tilde{\boldsymbol{x}}}_i =& -(\alpha+\beta_i)(\mathbf{I}_{df} - \boldsymbol{\Pi}_i)\tilde{\boldsymbol{x}}_i + (\mathbf{I}_{df} - \boldsymbol{\Pi}_i)\dot{\boldsymbol{\Pi}}_i\tilde{\boldsymbol{x}}_i\\ &-\boldsymbol{\Pi}_i\dot{\boldsymbol{x}}^* - k\boldsymbol{\Pi}_i\text{sgn}\left[\boldsymbol{\Pi}_i\sum_{j\in\mathcal{N}_i^f}(\tilde{\boldsymbol{x}}_i - \tilde{\boldsymbol{x}}_j)\right].\end{aligned} \tag{24}$$

In view of the fact $(\mathbf{I}_{df} - \boldsymbol{\Pi}_i) = \boldsymbol{0}_{df}$ for $i \in \boldsymbol{\mathcal{V}}_{f2}$, it is verified that (24) is satisfied by every follower $i \in \boldsymbol{\mathcal{V}}_f$.

Then, the error dynamics (24) is rewritten into the vector form, i.e.,

$$\begin{aligned}\dot{\tilde{\boldsymbol{x}}} =& -\left(\alpha\mathbf{I}_{dfn_f} + \mathbf{B}\right)\left(\mathbf{I}_{dfn_f} - \boldsymbol{\Pi}\right)\tilde{\boldsymbol{x}} - \left(\mathbf{I}_{dfn_f} - \boldsymbol{\Pi}\right)\dot{\boldsymbol{\Pi}}\tilde{\boldsymbol{x}}\\ &-\boldsymbol{\Pi}\dot{\boldsymbol{\chi}} - k\boldsymbol{\Pi}\text{sgn}\left(\boldsymbol{\Pi}\bar{\boldsymbol{\mathcal{L}}}_f\tilde{\boldsymbol{x}}\right),\end{aligned} \tag{25}$$

where

$$\begin{aligned}\bar{\boldsymbol{\mathcal{L}}}_f =&\boldsymbol{\mathcal{L}}_f \otimes \mathbf{I}_{df}\\ \tilde{\boldsymbol{x}} =&\left[\tilde{\boldsymbol{x}}_{n_l+1}^{\mathrm{T}} \quad \cdots \quad \tilde{\boldsymbol{x}}_n^{\mathrm{T}}\right]^{\mathrm{T}},\\ \dot{\boldsymbol{\chi}} =&\left[(\dot{\boldsymbol{x}}^*)^{\mathrm{T}} \quad \cdots \quad (\dot{\boldsymbol{x}}^*)^{\mathrm{T}}\right]^{\mathrm{T}},\\ \boldsymbol{\Pi} =&\text{diag}\left(\boldsymbol{\Pi}_{n_l+1}, \cdots, \boldsymbol{\Pi}_n\right),\\ \mathbf{B} =&\text{diag}\left(\beta_{n_l+1}, ..., \beta_n\right) \otimes \mathbf{I}_{df}.\end{aligned}$$

For step 3), we consider a Lyapunov function candidate

$$V_x(t) = \frac{1}{2}\tilde{\boldsymbol{x}}^{\mathrm{T}}\bar{\boldsymbol{\mathcal{L}}}_f\tilde{\boldsymbol{x}}.$$

It has $V_x(t) > 0$ except for the set of equilibrium $\left\{\tilde{\boldsymbol{x}} \in \mathbb{R}^{dfn_f} | \bar{\boldsymbol{\mathcal{L}}}_f\tilde{\boldsymbol{x}} = \boldsymbol{0}\right\}$. The set-valued Lie derivative of $V_x(t)$ with respect to (25) is given by

$$\begin{aligned}\mathcal{L}_{\text{Eq.}(25)}V_x(t) =&\tilde{\boldsymbol{x}}^{\mathrm{T}}\bar{\boldsymbol{\mathcal{L}}}_f\mathcal{F}\left\{\dot{\tilde{\boldsymbol{x}}}\right\}\\ =&-\left(\alpha\mathbf{I}_{dfn_f} + \mathbf{B}\right)\tilde{\boldsymbol{x}}^{\mathrm{T}}\bar{\boldsymbol{\mathcal{L}}}_f\left(\mathbf{I}_{dfn_f} - \boldsymbol{\Pi}\right)\tilde{\boldsymbol{x}}\\ &-\tilde{\boldsymbol{x}}^{\mathrm{T}}\bar{\boldsymbol{\mathcal{L}}}_f\left(\mathbf{I}_{dfn_f} - \boldsymbol{\Pi}\right)\dot{\boldsymbol{\Pi}}\tilde{\boldsymbol{x}}\\ &-\tilde{\boldsymbol{x}}^{\mathrm{T}}\bar{\boldsymbol{\mathcal{L}}}_f\boldsymbol{\Pi}\dot{\boldsymbol{\chi}} - k\tilde{\boldsymbol{x}}^{\mathrm{T}}\bar{\boldsymbol{\mathcal{L}}}_f\mathcal{F}\left\{\boldsymbol{\Pi}\text{sgn}\left(\boldsymbol{\Pi}\bar{\boldsymbol{\mathcal{L}}}_f\tilde{\boldsymbol{x}}\right)\right\}.\end{aligned}$$

According to Assumption 5, we also know $\|\dot{\boldsymbol{x}}^*\|_1 < \delta_1$. Therefore, for $\forall h \in -\tilde{\boldsymbol{x}}^{\mathrm{T}}\bar{\boldsymbol{\mathcal{L}}}_f\boldsymbol{\Pi}\dot{\boldsymbol{\chi}} - k\tilde{\boldsymbol{x}}^{\mathrm{T}}\bar{\boldsymbol{\mathcal{L}}}_f\mathcal{F}\left\{\boldsymbol{\Pi}\text{sgn}\left(\boldsymbol{\Pi}\bar{\boldsymbol{\mathcal{L}}}_f\tilde{\boldsymbol{x}}\right)\right\}$, it has

$$\begin{aligned}h \le& -(k-\delta_1)\sum_{i=1}^{n}\left\|\boldsymbol{\Pi}_i\sum_{j\in\mathcal{N}_i^f}(\tilde{\boldsymbol{x}}_i - \tilde{\boldsymbol{x}}_j)\right\|_1\\ \le& -(k-\delta_1)\left\|\boldsymbol{\Pi}\bar{\boldsymbol{\mathcal{L}}}_f\tilde{\boldsymbol{x}}\right\|_1.\end{aligned}$$

In view of Section II-D, $\dot{V}_x(t) \in \mathcal{L}_{\text{Eq.}(25)}V_x(t)$ for almost all $t \ge 0$. It gives

$$\begin{aligned}&\max\mathcal{L}_{\text{Eq.}(25)}V_x(t)\\ \le& -\tilde{\boldsymbol{x}}^{\mathrm{T}}\left(\alpha\mathbf{I}_{dfn_f} + \mathbf{B} - \dot{\boldsymbol{\Pi}}\right)\left(\mathbf{I}_{dfn_f} - \boldsymbol{\Pi}\right)\bar{\boldsymbol{\mathcal{L}}}_f\tilde{\boldsymbol{x}}\\ &-(k-\delta_1)\left\|\boldsymbol{\Pi}\bar{\boldsymbol{\mathcal{L}}}_f\tilde{\boldsymbol{x}}\right\|_1.\end{aligned}$$

Note that $\alpha\mathbf{I}_{dfn_f} + \mathbf{B} - \dot{\boldsymbol{\Pi}}$ is positive definite, because one observes that all eigenvalues of $\alpha\mathbf{I}_{dfn_f} + \mathbf{B} - \dot{\boldsymbol{\Pi}}$ are positive using the Gerschgorin disk theorem [41]. We also know $k > \delta_1$. Further, in view of Lemma 5, we know that both $\left(\mathbf{I}_{dfn_f} - \boldsymbol{\Pi}\right)$ and $\bar{\boldsymbol{\mathcal{L}}}_f$ are positive semi-definite. It concludes $\dot{V}_x(t) \le 0$.

When $\dot{V}_x(t) = 0$, it holds the following two conditions

$$\begin{aligned}\left(k\mathbf{I}_{dfn_f} + \mathbf{B} - \dot{\boldsymbol{\Pi}}\right)\left(\mathbf{I}_{dfn_f} - \boldsymbol{\Pi}\right)\bar{\boldsymbol{\mathcal{L}}}_f\tilde{\boldsymbol{x}} =&\boldsymbol{0}_{dfn_f},\\ \boldsymbol{\Pi}\bar{\boldsymbol{\mathcal{L}}}_f\tilde{\boldsymbol{x}} =&\boldsymbol{0}_{dfn_f}.\end{aligned}$$

There is no non-zero vector $\boldsymbol{\phi} = \bar{\boldsymbol{\mathcal{L}}}_f\tilde{\boldsymbol{x}}$ that satisfies both $\left(\mathbf{I}_{dfn_f} - \boldsymbol{\Pi}\right)\boldsymbol{\phi} = \boldsymbol{0}_{dfn_f}$ and $\boldsymbol{\Pi}\boldsymbol{\phi} = \boldsymbol{0}_{dfn_f}$, because the

corresponding null space of $\left(\mathbf{I}_{dfn_f}-\mathbf{\Pi}\right)$ and $\mathbf{\Pi}$ are complementary. Therefore, when $\dot{V}_x=0$, it must have $\bar{\boldsymbol{\mathcal{L}}}_f\tilde{\boldsymbol{x}}=\boldsymbol{0}_{dfn_f}$, which implies shape estimation errors $\{\tilde{\boldsymbol{x}}_i\}_{i\in\boldsymbol{\mathcal{V}}_f}$ can reach consensus, i.e., $\tilde{\boldsymbol{x}}_i(t)-\tilde{\boldsymbol{x}}_j(t)\to\boldsymbol{0}_f$, $t\to\infty$, $\forall i,j\in\boldsymbol{\mathcal{V}}_f$. Furthermore, we have $\boldsymbol{x}_i(t)-\boldsymbol{x}_j(t)\to\boldsymbol{0}_f$, $t\to\infty$, $\forall i,j\in\boldsymbol{\mathcal{V}}_f$. It means local shape estimations will also reach the consensus. The proof is completed. ■

In view of Theorems 2 and 3, we know that local estimations $\{\boldsymbol{x}_i(t)\}_{i\in\boldsymbol{\mathcal{V}}_f}$ will converge to their corresponding time-varying manifolds $\boldsymbol{\mathcal{M}}_i(t)$ in finite time and reach consensus eventually. It implies that local estimation $\boldsymbol{x}_i(t)$ is able to achieve the designed two sub-objectives. Therefore, these local estimations can cooperatively obtain the unique solution of the time-varying linear equation (12). Here, we have the following proposition to conclude the performance of the estimator (13).

Proposition 1: Under Assumptions 1-6, for all followers, the estimator (13) can let $\boldsymbol{x}_i(t)$ with the dynamics (10) to track $\boldsymbol{x}^*(t)$, i.e.,

$$\lim_{t\to\infty}\left[\boldsymbol{x}_i(t)-\boldsymbol{x}^*(t)\right]=\boldsymbol{0}_{df},\qquad\forall i\in\boldsymbol{\mathcal{V}}_f.$$

V. Cooperative Formation Translation Estimator Design

This section describes a distributed method for followers to cooperatively estimate the formation translation $\boldsymbol{y}^*(t)$. We make the following assumption regarding the boundness of the variable.

Assumption 7: The derivative of $\boldsymbol{y}^*(t)$ is bounded by $||\dot{\boldsymbol{y}}^*(t)||_2<\delta_3$, where $\delta_3>0$.

Let $\boldsymbol{y}_i(t)\in\mathbb{R}^{df}$ represent the local estimation of $\boldsymbol{y}^*(t)$ for follower i. It satisfies the following integrator dynamics

$$\dot{\boldsymbol{y}}_i(t)=\boldsymbol{\eta}_i(t),\qquad i\in\boldsymbol{\mathcal{V}}_f,\tag{26}$$

where $\boldsymbol{\eta}_i(t)\in\mathbb{R}^d$ is designed as

$$\begin{aligned}&\boldsymbol{\eta}_i(t)\\&=-\frac{\sigma_1}{\left|\boldsymbol{\mathcal{N}}_i^l\right|}\sum_{j\in\boldsymbol{\mathcal{N}}_i^l}\left(\boldsymbol{y}_i(t)-\boldsymbol{p}_j(t)+\left(\boldsymbol{r}_j^{\mathrm{T}}(t)\otimes\mathbf{I}_d\right)\boldsymbol{x}_i(t)\right)\\&\quad-\frac{\sigma_2}{\left|\boldsymbol{\mathcal{N}}_i^l\right|}\mathrm{sgn}\left[\sum_{j\in\boldsymbol{\mathcal{N}}_i^l}\left(\boldsymbol{y}_i(t)-\boldsymbol{p}_j(t)+\left(\boldsymbol{r}_j^{\mathrm{T}}(t)\otimes\mathbf{I}_d\right)\boldsymbol{x}_i(t)\right)\right]\\&\quad-\sigma_3\mathrm{sgn}\left[\sum_{j\in\boldsymbol{\mathcal{N}}_i^f}\left(\boldsymbol{y}_i(t)-\boldsymbol{y}_j(t)\right)\right],\end{aligned}\tag{27}$$

where $\sigma_1>0$, $\sigma_2>n_f\delta_3$, $\sigma_3>0$.

The translation estimation error is defined as

$$\tilde{\boldsymbol{y}}_i(t)\triangleq\boldsymbol{y}_i(t)-\boldsymbol{y}^*(t)=\boldsymbol{y}_i(t)-\boldsymbol{p}_j^*(t)+\left(\boldsymbol{r}_j^{\mathrm{T}}(t)\otimes\mathbf{I}_d\right)\boldsymbol{x}^*(t),$$

where $j\in\boldsymbol{\mathcal{V}}_l$ denotes any one leader.

The error dynamics of translation estimation are given by

$$\begin{aligned}&\dot{\tilde{\boldsymbol{y}}}_i(t)\\&=\boldsymbol{\eta}_i(t)-\dot{\boldsymbol{y}}_i^*(t)\\&=-\frac{\sigma_1}{\left|\boldsymbol{\mathcal{N}}_i^l\right|}\sum_{j\in\boldsymbol{\mathcal{N}}_i^l}\left(\tilde{\boldsymbol{y}}_i(t)-\tilde{\boldsymbol{p}}_j(t)+\left(\boldsymbol{r}_i^{\mathrm{T}}(t)\otimes\mathbf{I}_d\right)\tilde{\boldsymbol{x}}_i(t)\right)\\&\quad-\frac{\sigma_2}{\left|\boldsymbol{\mathcal{N}}_i^l\right|}\mathrm{sgn}\left[\sum_{j\in\boldsymbol{\mathcal{N}}_i^l}\left(\tilde{\boldsymbol{y}}_i(t)-\tilde{\boldsymbol{p}}_j(t)+\left(\boldsymbol{r}_j^{\mathrm{T}}(t)\otimes\mathbf{I}_d\right)\tilde{\boldsymbol{x}}_i(t)\right)\right]\\&\quad-\sigma_3\mathrm{sgn}\left[\sum_{j\in\boldsymbol{\mathcal{N}}_i^f}\left(\tilde{\boldsymbol{y}}_i(t)-\tilde{\boldsymbol{y}}_j(t)\right)\right]-\dot{\boldsymbol{y}}_i^*(t).\end{aligned}\tag{28}$$

Now, we define the following cascaded time-varying systems:

$$\Sigma_1:\dot{\tilde{\boldsymbol{y}}}=\boldsymbol{\varrho}_1\left(t,\tilde{\boldsymbol{y}},\tilde{\boldsymbol{p}}_l,\tilde{\boldsymbol{x}}\right),\tag{29}$$

$$\Sigma_2:\begin{cases}\dot{\tilde{\boldsymbol{p}}}_l=\boldsymbol{\varrho}_{21}\left(t,\tilde{\boldsymbol{p}}_l\right)\\\dot{\tilde{\boldsymbol{x}}}=\boldsymbol{\varrho}_{22}\left(t,\tilde{\boldsymbol{x}}\right)\end{cases},\tag{30}$$

where Σ_1 represents the error dynamics of translation estimation. Σ_2 comprises dynamics of leaders' position error and shape estimation error.

We first study the stability of the system Σ_1 under the condition that $(\tilde{\boldsymbol{p}}_l,\tilde{\boldsymbol{x}})=\left(\boldsymbol{0}_{dn_l},\boldsymbol{0}_{dfn_f}\right)$. Then, Σ_1 becomes

$$\dot{\tilde{\boldsymbol{y}}}(t)=\boldsymbol{\varrho}_1\left(t,\tilde{\boldsymbol{y}},\boldsymbol{0}_{dn_l},\boldsymbol{0}_{dfn_f}\right).\tag{31}$$

Furthermore, error dynamics of translation estimation (28) becomes

$$\begin{aligned}\dot{\tilde{\boldsymbol{y}}}_i(t)=&-\sigma_1\tilde{\boldsymbol{y}}_i(t)-\sigma_2\mathrm{sgn}\left(\tilde{\boldsymbol{y}}_i(t)\right)\\&-\sigma_3\mathrm{sgn}\left[\sum_{j\in\boldsymbol{\mathcal{N}}_i^f}\left(\tilde{\boldsymbol{y}}_i(t)-\tilde{\boldsymbol{y}}_j(t)\right)\right]-\dot{\boldsymbol{y}}_i^*(t).\end{aligned}$$

Thus, eq.(31) is expressed as

$$\begin{aligned}\dot{\tilde{\boldsymbol{y}}}(t)=&-\sigma_1\tilde{\boldsymbol{y}}(t)-\sigma_2\mathrm{sgn}\left(\tilde{\boldsymbol{y}}(t)\right)\\&-\sigma_3\mathrm{sgn}\left(\hat{\boldsymbol{\mathcal{L}}}_f\tilde{\boldsymbol{y}}(t)\right)-\dot{\boldsymbol{\kappa}}(t),\end{aligned}\tag{32}$$

where $\hat{\boldsymbol{\mathcal{L}}}_f=\boldsymbol{\mathcal{L}}_f\otimes\mathbf{I}_d$, and

$$\begin{aligned}\tilde{\boldsymbol{y}}(t)&=\left[\tilde{\boldsymbol{y}}_{n_l+1}^{\mathrm{T}}(t)\quad\cdots\quad\tilde{\boldsymbol{y}}_n^{\mathrm{T}}(t)\right]^{\mathrm{T}},\\\dot{\boldsymbol{\kappa}}(t)&=\left[\left(\dot{\boldsymbol{y}}^*(t)\right)^{\mathrm{T}}\quad\cdots\quad\left(\dot{\boldsymbol{y}}^*(t)\right)^{\mathrm{T}}\right]^{\mathrm{T}}.\end{aligned}$$

Theorem 4: Under Assumptions 1 and 2, the translation estimation error $\tilde{\boldsymbol{y}}_i$ with the dynamics described by (32) will reach consensus in finite time T_{Ly}, i.e.

$$\lim_{t\to T_{Ly}}\left[\tilde{\boldsymbol{y}}_i(t)-\tilde{\boldsymbol{y}}_j(t)\right]=\boldsymbol{0}_d,\qquad\forall i,j\in\boldsymbol{\mathcal{V}}_f,$$

where

$$T_{Ly}=\frac{V_{Ly}^{\frac{1}{2}}(0)}{2\sigma_3\lambda_2\left(\boldsymbol{\mathcal{L}}_{\boldsymbol{f}}\right)},$$

$$V_{Ly}(t)=\frac{1}{2}\tilde{\boldsymbol{y}}^{\mathrm{T}}(t)\hat{\boldsymbol{\mathcal{L}}}_f\tilde{\boldsymbol{y}}(t).$$

Proof: We consider the Lyapunov function candidate $V_{Ly}(t)=\frac{1}{2}\tilde{\boldsymbol{y}}^{\mathrm{T}}(t)\hat{\boldsymbol{\mathcal{L}}}_f\tilde{\boldsymbol{y}}(t)$. It has $V_{Ly}(t)>0$ except for the

set of equilibrium $\left\{\tilde{\boldsymbol{y}} \in \mathbb{R}^{dn_f} | \hat{\boldsymbol{\mathcal{L}}}_f \tilde{\boldsymbol{y}} = \boldsymbol{0}\right\}$. The set-valued Lie derivative of $V_{Ly}(t)$ with respect to (32) is given by

$$\begin{aligned}
&\mathcal{L}_{\text{Eq.}(32)} V_{Ly}(t) \\
=&\tilde{\boldsymbol{y}}^{\mathrm{T}}(t) \hat{\boldsymbol{\mathcal{L}}}_f \mathcal{F}\left\{\dot{\tilde{\boldsymbol{y}}}(t)\right\} \\
=&-\sigma_1 \tilde{\boldsymbol{y}}^{\mathrm{T}}(t) \hat{\boldsymbol{\mathcal{L}}}_f \tilde{\boldsymbol{y}}(t) - \tilde{\boldsymbol{y}}^{\mathrm{T}}(t) \boldsymbol{\mathcal{L}}_f \dot{\boldsymbol{\kappa}}(t) \\
&-\tilde{\boldsymbol{y}}^{\mathrm{T}}(t) \hat{\boldsymbol{\mathcal{L}}}_f \mathcal{F}\left\{\sigma_2 \operatorname{sgn}\left(\tilde{\boldsymbol{y}}(t)\right) + \sigma_3 \operatorname{sgn}\left(\hat{\boldsymbol{\mathcal{L}}}_f \tilde{\boldsymbol{y}}(t)\right)\right\}.
\end{aligned}$$

For $\forall h \in -\tilde{\boldsymbol{y}}^{\mathrm{T}}(t) \hat{\boldsymbol{\mathcal{L}}}_f \mathcal{F}\left\{\sigma_3 \operatorname{sgn}\left(\hat{\boldsymbol{\mathcal{L}}}_f \tilde{\boldsymbol{y}}(t)\right)\right\}$, it has $h \leq -\sigma_3 \left\|\hat{\boldsymbol{\mathcal{L}}}_f \tilde{\boldsymbol{y}}(t)\right\|_1$. Furthermore, it is analyzed that

$$\begin{aligned}
&\sigma_3 \tilde{\boldsymbol{y}}^{\mathrm{T}}(t) \hat{\boldsymbol{\mathcal{L}}}_f \operatorname{sgn}\left(\hat{\boldsymbol{\mathcal{L}}}_f \tilde{\boldsymbol{y}}(t)\right) \\
=&-\sum_{i \in \boldsymbol{\mathcal{V}}_f} \frac{1}{\left|\boldsymbol{\mathcal{N}}_i^l\right|} \sum_{j \in \boldsymbol{\mathcal{N}}_i^l} \tilde{\boldsymbol{y}}_i^{\mathrm{T}}(t) \left[\operatorname{sgn}\left(\tilde{\boldsymbol{y}}_i(t)\right) - \operatorname{sgn}\left(\tilde{\boldsymbol{y}}_j(t)\right)\right] \leq 0.
\end{aligned}$$

Therefore, for $\forall s \in -\tilde{\boldsymbol{y}}^{\mathrm{T}}(t) \boldsymbol{\Xi} \mathcal{F}\left\{\operatorname{sgn}\left(\tilde{\boldsymbol{y}}(t)\right)\right\}$, it has $s \leq 0$, where $\boldsymbol{\Xi} = \mathbf{I}_{dn_f} - \frac{1}{n_f} \boldsymbol{I}_{dn_f} \boldsymbol{I}_{dn_f}^{\mathrm{T}}$. It satisfies $\hat{\boldsymbol{\mathcal{L}}}_f \geq \lambda_2\left(\boldsymbol{\mathcal{L}}_f\right) \boldsymbol{\Xi}$, and $\boldsymbol{\Xi}^2 = \boldsymbol{\Xi}$.

In view of Section II-D, $\dot{V}_{Ly}(t) \in \mathcal{L}_{\text{Eq.}(32)} V_{Ly}(t)$ for almost all $t \geq 0$. Then, by combining with the fact $\boldsymbol{\Xi} \dot{\boldsymbol{\kappa}} = \boldsymbol{0}_{dn_f}$, it follows

$$\max \mathcal{L}_{\text{Eq.}(32)} V_{Ly}(t) \leq -\sigma_3 \left\|\hat{\boldsymbol{\mathcal{L}}}_f \tilde{\boldsymbol{y}}(t)\right\|_1 \leq -4\sigma_3 \lambda_2\left(\boldsymbol{\mathcal{L}}_f\right) V_y^{\frac{1}{2}}(t).$$

In view of Lemma 2, it follows $\hat{\boldsymbol{\mathcal{L}}}_f \tilde{\boldsymbol{y}}(t) \to \boldsymbol{0}_{dn_f}$, $t \to T_{Ly}$. It implies $\tilde{\boldsymbol{y}}_i(t) - \tilde{\boldsymbol{y}}_j(t) \to \boldsymbol{0}_d$, $\forall i, j \in \boldsymbol{\mathcal{V}}_f$, $t \to T_{Ly}$. ■

Theorem 5: Under Assumptions 1, 2, and 7, the estimation error $\tilde{\boldsymbol{y}}_i(t)$ with the dynamics described by (32) will converge to zero in finite time T_y, i.e.,

$$\lim_{t \to T_y} \tilde{\boldsymbol{y}}_i(t) = \boldsymbol{0}_d, \qquad \forall i \in \boldsymbol{\mathcal{V}}_f,$$

where

$$\begin{aligned}
T_y =& T_{Ly} + \frac{1}{\sigma_1} \ln \frac{\sigma_1 \hat{V}_y^{\frac{1}{2}} - 2\left(\sigma_2 - \delta_3\right)}{2\left(\sigma_2 - \delta_3\right)}, \\
\hat{V}_y =& \sup_{\tau \in [0, T_{Ly}]} V_y(\tau), \\
V_y(t) =& \frac{1}{2} \tilde{\boldsymbol{y}}^{\mathrm{T}}(t) \tilde{\boldsymbol{y}}(t).
\end{aligned}$$

Proof: In view of Theorem 4, when $t > T_y$, it has

$$\bar{\boldsymbol{\mathcal{L}}}_f \tilde{\boldsymbol{y}}(t) = \boldsymbol{0}_{dn_f}.$$

We consider the Lyapunov function candidate $V_y(t) = \frac{1}{2} \tilde{\boldsymbol{y}}^{\mathrm{T}}(t) \tilde{\boldsymbol{y}}(t)$. When $t > T_y$, the set-valued Lie derivative of $V_y(t)$ with respect to (32) is given by

$$\begin{aligned}
\mathcal{L}_{\text{Eq.}(32)} V_y(t) =& \tilde{\boldsymbol{y}}^{\mathrm{T}}(t) \mathcal{F}\left\{\dot{\tilde{\boldsymbol{y}}}(t)\right\} \\
=& \tilde{\boldsymbol{y}}^{\mathrm{T}}(t) \mathcal{F}\left\{-\sigma_1 \tilde{\boldsymbol{y}}(t) - \sigma_2 \operatorname{sgn}\left(\tilde{\boldsymbol{y}}(t)\right) + \dot{\boldsymbol{\kappa}}(t)\right\}.
\end{aligned}$$

According to Assumption 7, it is also known that $\|\dot{\boldsymbol{y}}^*(t)\|_2 \leq \delta_3$. Therefore, for $\forall h \in -\tilde{\boldsymbol{y}}^{\mathrm{T}}(t) \mathcal{F}\left\{\sigma_2 \operatorname{sgn}\left(\tilde{\boldsymbol{y}}(t)\right) + \dot{\boldsymbol{\kappa}}(t)\right\}$, it has $h \leq -\left(\sigma_2 - \delta_3\right) \|\tilde{\boldsymbol{y}}(t)\|_1$. In view of Section II-D, $\dot{V}_y(t) \in \mathcal{L}_{\text{Eq.}(32)} V_y(t)$ for almost all $t \geq 0$. It has

$$\begin{aligned}
\max \mathcal{L}_{\text{Eq.}(32)} V_y(t) \leq& -\sigma_1 \tilde{\boldsymbol{y}}^{\mathrm{T}}(t) \tilde{\boldsymbol{y}}(t) - \left(\sigma_2 - \delta_3\right) \|\tilde{\boldsymbol{y}}(t)\|_1 \\
\leq& -2\sigma_1 V_y(t) - 4\left(\sigma_2 - \delta_3\right) V_y^{\frac{1}{2}}(t).
\end{aligned}$$

In view of Lemma 1, it follows $\tilde{\boldsymbol{y}}_i(t) \to \boldsymbol{0}_d$, $t \to T_y$. ■

Theorem 5 shows that the system Σ_1 is UGAS under the condition $(\tilde{\boldsymbol{p}}_l, \tilde{\boldsymbol{x}}) = \left(\boldsymbol{0}_{dn_l}, \boldsymbol{0}_{dfn_f}\right)$. Here we have the following proposition to conclude the stability of system Σ_1 combining with the shape estimator described in the previous section.

Proposition 2: Under Assumptions 1-7, the estimator (27) can let local translation estimation $\boldsymbol{y}_i(t)$ converge to $\boldsymbol{y}^*(t)$, i.e.,

$$\lim_{t \to \infty} \tilde{\boldsymbol{y}}_i(t) = \boldsymbol{0}_d, \qquad \forall i \in \boldsymbol{\mathcal{V}}_f.$$

Proof: In view of Proposition 1, it has $\lim_{t \to \infty} \tilde{\boldsymbol{x}}(t) = \boldsymbol{0}_{dfn_f}$. Combing with $\lim_{t \to \infty} \tilde{\boldsymbol{p}}_l(t) = \boldsymbol{0}_{dn_l}$, we know that the system Σ_2 is t_0-uniformly bounded and UGAS with the equilibrium $(\tilde{\boldsymbol{p}}_l, \tilde{\boldsymbol{x}}) = \left(\boldsymbol{0}_{dn_l}, \boldsymbol{0}_{dfn_f}\right)$.

From Theorem 5, we know the equilibrium $\tilde{\boldsymbol{y}}(t) = \boldsymbol{0}_{dn_f}$ is UGAS for the system (31). Further, the system Σ_1 is also t_0-uniformly bounded, because $\boldsymbol{y}_i^*(t)$, $\tilde{\boldsymbol{p}}_l(t)$, and $\tilde{\boldsymbol{x}}_i(t)$ are all bounded.

Therefore, according to Lemma 3, the system Σ_1 with the equilibrium $(\tilde{\boldsymbol{y}}, \tilde{\boldsymbol{p}}_l, \tilde{\boldsymbol{x}}) = \left(\boldsymbol{0}_{dn_f}, \boldsymbol{0}_{dn_l}, \boldsymbol{0}_{dfn_f}\right)$ is UGAS, which implies $\lim_{t \to \infty} \tilde{\boldsymbol{y}}_i(t) = \boldsymbol{0}_d$, $\forall i \in \boldsymbol{\mathcal{V}}_f$. ■

VI. Time-varying Linear Formation Tracking Controller Design

This section describes a cooperative linear formation tracking control method for followers to track their desired positions $\boldsymbol{p}_f^*(t)$ using the estimated shape and translation parameters $\boldsymbol{x}_i(t)$ and $\boldsymbol{y}_i(t)$.

For followers with dynamics (5), the linear formation tracking control law is designed as follows:

$$\begin{aligned}
\boldsymbol{u}_i(t) =& \left(\dot{\boldsymbol{r}}_i^{\mathrm{T}}(t) \otimes \mathbf{I}_d\right) \boldsymbol{x}_i(t) + \left(\boldsymbol{r}_i^{\mathrm{T}}(t) \otimes \mathbf{I}_d\right) \dot{\boldsymbol{x}}_i(t) + \dot{\boldsymbol{y}}_i(t) \\
&- \rho\left[\boldsymbol{p}_i(t) - \left(\boldsymbol{r}_i^{\mathrm{T}}(t) \otimes \mathbf{I}_d\right) \boldsymbol{x}_i(t) - \boldsymbol{y}_i(t)\right],
\end{aligned} \tag{33}$$

where $\rho > 0$.

The follower's position error is defined as $\tilde{\boldsymbol{p}}_i(t) \triangleq \boldsymbol{p}_i(t) - \boldsymbol{p}_i^*(t)$, $\forall i \in \boldsymbol{\mathcal{V}}_f$.

The derivative of $\boldsymbol{p}_i^*(t)$ is obtained by

$$\dot{\boldsymbol{p}}_i^*(t) = \dot{\boldsymbol{y}}^*(t) + \left(\dot{\boldsymbol{r}}_i^{\mathrm{T}}(t) \otimes \mathbf{I}_d\right) \boldsymbol{x}^*(t) + \left(\boldsymbol{r}_i^{\mathrm{T}}(t) \otimes \mathbf{I}_d\right) \dot{\boldsymbol{x}}^*(t).$$

Then, the position error dynamics are obtained by

$$\begin{aligned}
\dot{\tilde{\boldsymbol{p}}}_i(t) =& \left(\dot{\boldsymbol{r}}_i^{\mathrm{T}}(t) \otimes \mathbf{I}_d\right) \tilde{\boldsymbol{x}}_i(t) + \left(\boldsymbol{r}_i^{\mathrm{T}}(t) \otimes \mathbf{I}_d\right) \dot{\tilde{\boldsymbol{x}}}_i(t) + \dot{\tilde{\boldsymbol{y}}}_i(t) \\
&- \rho \tilde{\boldsymbol{p}}_i(t) + \rho\left(\boldsymbol{r}_i^{\mathrm{T}}(t) \otimes \mathbf{I}_d\right) \tilde{\boldsymbol{x}}_i(t) + \rho \tilde{\boldsymbol{y}}_i(t).
\end{aligned} \tag{34}$$

Now, we define the following cascaded time-varying systems:

$$\Sigma_3 : \dot{\tilde{\boldsymbol{p}}}_f = \boldsymbol{\varrho}_3\left(t, \tilde{\boldsymbol{p}}_f, \tilde{\boldsymbol{x}}, \dot{\tilde{\boldsymbol{x}}}, \tilde{\boldsymbol{y}}, \dot{\tilde{\boldsymbol{y}}}\right), \tag{35}$$

$$\Sigma_4 : \begin{cases} \ddot{\tilde{\boldsymbol{x}}} = \boldsymbol{\varrho}_{41}\left(t, \tilde{\boldsymbol{x}}, \dot{\tilde{\boldsymbol{x}}}\right) \\ \ddot{\tilde{\boldsymbol{y}}} = \boldsymbol{\varrho}_{42}\left(t, \tilde{\boldsymbol{y}}, \dot{\tilde{\boldsymbol{y}}}\right) \end{cases}, \tag{36}$$

where Σ_3 represents the dynamics of followers' position error. Σ_4 comprises the error dynamics of shape and translation estimations.

Theorem 6: Under Assumptions 1-7, the formation tracking controller (33) can let followers with the dynamics (5) to track the target formation $\boldsymbol{p}_i^*(t)$, i.e.,

$$\lim_{t\to\infty}\tilde{\boldsymbol{p}}_i(t)=\boldsymbol{0}_d,\qquad \forall i\in\boldsymbol{\mathcal{V}}_f.$$

Proof: We first study the stability of the system Σ_3 under the condition $\left(\tilde{\boldsymbol{x}},\dot{\tilde{\boldsymbol{x}}},\tilde{\boldsymbol{y}},\dot{\tilde{\boldsymbol{y}}}\right)=\left(\boldsymbol{0}_{dfn_f},\boldsymbol{0}_{dfn_f},\boldsymbol{0}_{dn_f},\boldsymbol{0}_{dn_f}\right)$. Then, Σ_3 becomes

$$\dot{\tilde{\boldsymbol{p}}}_f=\boldsymbol{\varrho}_3\left(t,\tilde{\boldsymbol{p}}_f,\boldsymbol{0}_{dfn_f},\boldsymbol{0}_{dfn_f},\boldsymbol{0}_{dn_f},\boldsymbol{0}_{dn_f}\right). \tag{37}$$

We consider the following Lyapunov function candidate for (37):

$$V_p(t)=\frac{1}{2}\tilde{\boldsymbol{p}}_f^{\mathrm{T}}(t)\tilde{\boldsymbol{p}}_f(t),$$

whose derivative is given by $\dot{V}_p=\tilde{\boldsymbol{p}}_f^{\mathrm{T}}\dot{\tilde{\boldsymbol{p}}}_f=-\rho\tilde{\boldsymbol{p}}_f^{\mathrm{T}}\tilde{\boldsymbol{p}}_f$.

Therefore, the system (37) is UGAS with the equilibrium $\tilde{\boldsymbol{p}}_f(t)=\boldsymbol{0}_{dn_f}$.

In view of Propositions 1 and 2, we know $\lim_{t\to\infty}\tilde{\boldsymbol{x}}(t)=\boldsymbol{0}_{dfn_f}$, and $\lim_{t\to\infty}\tilde{\boldsymbol{y}}(t)=\boldsymbol{0}_{dn_f}$. Further, it apparently has $\lim_{t\to\infty}\dot{\tilde{\boldsymbol{x}}}(t)=\boldsymbol{0}_{dfn_f}$, and $\lim_{t\to\infty}\dot{\tilde{\boldsymbol{y}}}(t)=\boldsymbol{0}_{dn_f}$. Thus, the system Σ_4 is t_0-uniformly bounded and UGAS with the equilibrium $\left(\tilde{\boldsymbol{x}},\dot{\tilde{\boldsymbol{x}}},\tilde{\boldsymbol{y}},\dot{\tilde{\boldsymbol{y}}}\right)=\left(\boldsymbol{0}_{dfn_f},\boldsymbol{0}_{dfn_f},\boldsymbol{0}_{dn_f},\boldsymbol{0}_{dn_f}\right)$.

Combing with the fact that the system (37) is UGAS with the equilibrium $\tilde{\boldsymbol{p}}_f(t)=\boldsymbol{0}_{dn_f}$, we know the system Σ_3 is also t_0-uniformly bounded, because $\tilde{\boldsymbol{x}}_i(t)$, $\dot{\tilde{\boldsymbol{x}}}_i(t)$, $\tilde{\boldsymbol{y}}_i(t)$, and $\dot{\tilde{\boldsymbol{y}}}_i(t)$ are all bounded.

Therefore, according to Lemma 3, the system Σ_3 with the equilibrium $\left(\tilde{\boldsymbol{p}}_f,\tilde{\boldsymbol{x}},\dot{\tilde{\boldsymbol{x}}},\tilde{\boldsymbol{y}},\dot{\tilde{\boldsymbol{y}}}\right)=\left(\boldsymbol{0}_{dn_f},\boldsymbol{0}_{dfn_f},\boldsymbol{0}_{dfn_f},\boldsymbol{0}_{dn_f},\boldsymbol{0}_{dn_f}\right)$ is UGAS, which implies $\lim_{t\to\infty}\tilde{\boldsymbol{p}}_i(t)=\boldsymbol{0}_d$, $\forall i\in\boldsymbol{\mathcal{V}}_f$. ■

VII. Simulation

This section presents simulation results to verify the estimation-based time-varying linear formation tracking control schemes. The desired time-varying formation is generated by the optimization-based method described in Appendix A.

A. Simulation Setup

We consider a formation maneuver task in $\mathbb{R}^2$. There is a group of 16 agents, including 5 leaders and 11 followers. The communication topology among agents is given in Fig. 3. The subgraph within followers is undirected and connected. Thereby, Assumption 1 is satisfied.

The time-varying nominal configuration $\{\boldsymbol{r}_i(t)\}_{i=1}^{16}$ is a scaling hypercube lying in $\mathbb{R}^4$. It satisfies the following dynamics

$$\dot{\boldsymbol{r}}_i(t)=0.04\cos(0.1t)\,\boldsymbol{1}_4,$$

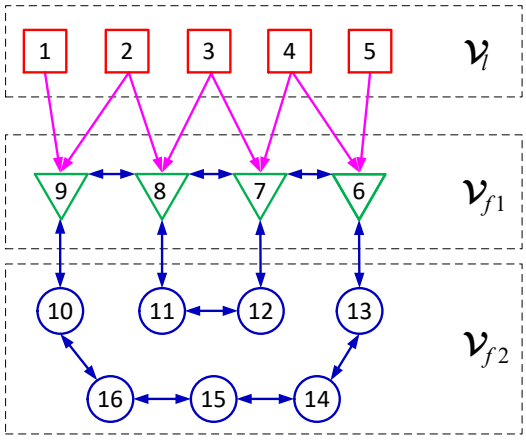

Fig. 3. Communication topology among agents. It is seen $\boldsymbol{\mathcal{V}_l}$ = {1, 2, 3, 4, 5}, $\boldsymbol{\mathcal{V}_{f1}}$ = {6, 7, 8, 9}, and $\boldsymbol{\mathcal{V}_{f2}}$ = {10, 11, 12, 13, 14, 15, 16}.

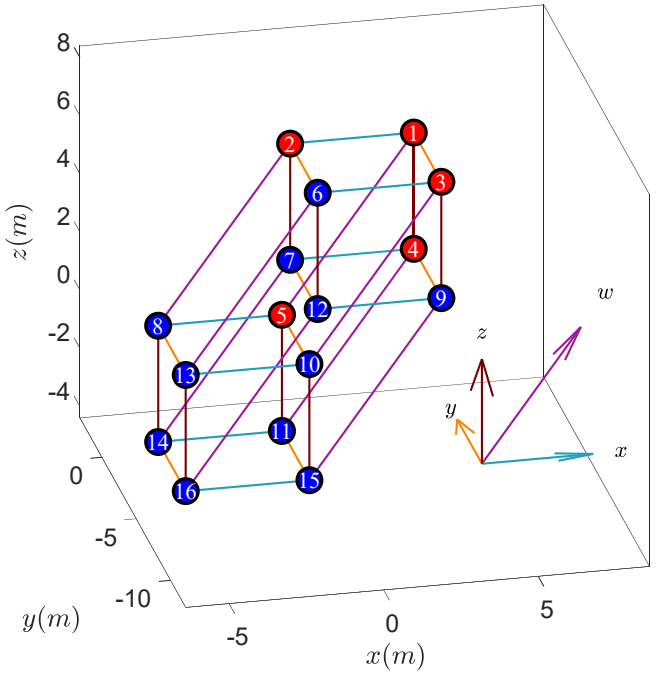

Fig. 4. A 4-dimensional hypercube is projected onto a 3-dimensional space. $\boldsymbol{x}$, $\boldsymbol{y}$, $\boldsymbol{z}$, and $\boldsymbol{w}$ are 4 coordinate axes of $\mathbb{R}^4$. The transformed coordinate axes are also presented. Note that straight lines connecting two agents in this figure do not represent a connected topology, but only represent edges parallel to the 4 coordinate axes.

with the initial value given by

$$\begin{aligned}
\boldsymbol{r}_1(0)&=\begin{bmatrix}2&2&2&2\end{bmatrix}^T & \boldsymbol{r}_2(0)&=\begin{bmatrix}-2&2&2&2\end{bmatrix}^T\\
\boldsymbol{r}_3(0)&=\begin{bmatrix}2&-2&2&2\end{bmatrix}^T & \boldsymbol{r}_4(0)&=\begin{bmatrix}2&2&-2&2\end{bmatrix}^T\\
\boldsymbol{r}_5(0)&=\begin{bmatrix}2&2&2&-2\end{bmatrix}^T & \boldsymbol{r}_6(0)&=\begin{bmatrix}-2&-2&2&2\end{bmatrix}^T\\
\boldsymbol{r}_7(0)&=\begin{bmatrix}-2&2&-2&2\end{bmatrix}^T & \boldsymbol{r}_8(0)&=\begin{bmatrix}-2&2&2&-2\end{bmatrix}^T\\
\boldsymbol{r}_9(0)&=\begin{bmatrix}2&-2&-2&2\end{bmatrix}^T & \boldsymbol{r}_{10}(0)&=\begin{bmatrix}2&-2&2&-2\end{bmatrix}^T\\
\boldsymbol{r}_{11}(0)&=\begin{bmatrix}2&2&-2&-2\end{bmatrix}^T & \boldsymbol{r}_{12}(0)&=\begin{bmatrix}-2&-2&-2&2\end{bmatrix}^T\\
\boldsymbol{r}_{13}(0)&=\begin{bmatrix}-2&-2&2&-2\end{bmatrix}^T & \boldsymbol{r}_{14}(0)&=\begin{bmatrix}-2&2&-2&-2\end{bmatrix}^T\\
\boldsymbol{r}_{15}(0)&=\begin{bmatrix}2&-2&-2&-2\end{bmatrix}^T & \boldsymbol{r}_{16}(0)&=\begin{bmatrix}-2&-2&-2&2\end{bmatrix}^T
\end{aligned}$$

It is verified that this time-varying nominal configuration with the interactive topology (shown in Fig. 3) always satisfies Assumptions 2 and 3. Fig. 4 shows the projection of the hypercube $\{\boldsymbol{r}_i(0)\}_{i=1}^{16}$, where the coordinates transformation

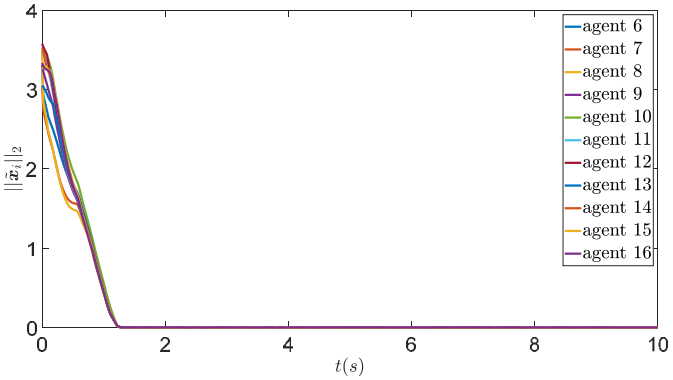

Fig. 5. Shape estimation errors.

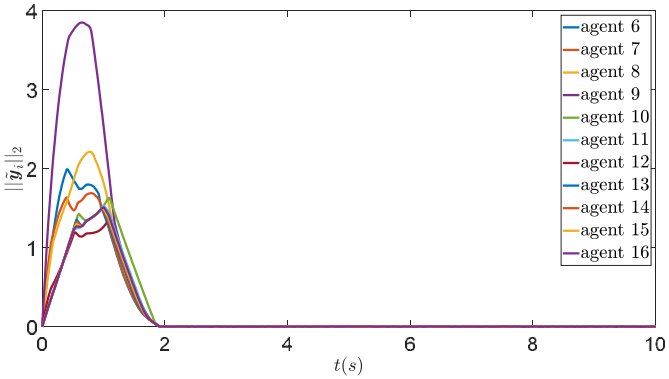

Fig. 6. Translation estimation errors.

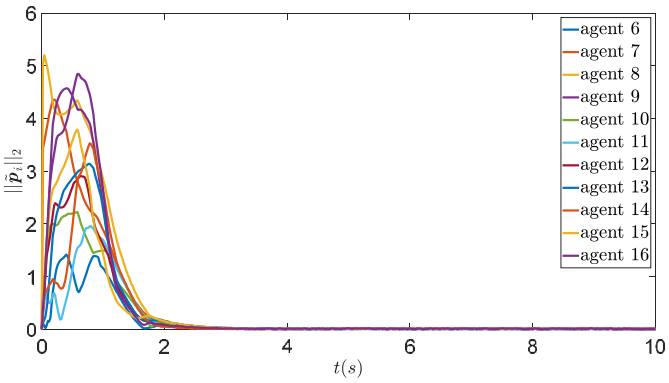

Fig. 7. Formation tracking errors.

matrix is given by

$$\begin{bmatrix} 1 & 0 & 0 & 1 \\ 0 & 1 & 0 & 0.5 \\ 0 & 0 & 1 & 1 \end{bmatrix}.$$

Two obstacles are modeled as planar circles with the same radius 6 m. Therefore, the safe distance is $l_k = 6$m. Their location are $\boldsymbol{q}_1 = \begin{bmatrix} 20 & 8 \end{bmatrix}^{\mathrm{T}}$m and $\boldsymbol{q}_2 = \begin{bmatrix} 18 & -8 \end{bmatrix}^{\mathrm{T}}$m, respectively. We select the safe distance among agents to be $l = 0.5$m. The gain matrix is set as $\mathbf{Q} = \mathrm{diag}\,(4\mathbf{I}_8, 2\mathbf{I}_2)$. The reference time-varying linear formation transformation parameters $\mathrm{vec}\left(\bar{\mathbf{A}}^{\mathrm{ref}}(t)\right)$ are selected satisfying the following dynamics

$$\mathrm{vec}\left(\dot{\bar{\mathbf{A}}}^{\mathrm{ref}}(t)\right) = \left[\left(\dot{\boldsymbol{x}}^{\mathrm{ref}}(t)\right)^{\mathrm{T}} \quad \left(\dot{\boldsymbol{y}}^{\mathrm{ref}}(t)\right)^{\mathrm{T}}\right]^{\mathrm{T}},$$

$$\dot{\boldsymbol{x}}^{\mathrm{ref}}(t) = -\frac{0.04\cos(0.1t)}{0.16\sin^2(0.1t)}\boldsymbol{I}_8,$$

$$\dot{\boldsymbol{y}}^{\mathrm{ref}}(t) = \begin{cases} \begin{bmatrix} 0.4 & 0 \end{bmatrix}^{\mathrm{T}} & 10s \le t \le 110s \\ \boldsymbol{0}_2 & \text{other} \end{cases},$$

with the initial value

$$\bar{\mathbf{A}}^{\mathrm{ref}}(0) = \begin{bmatrix} 1.2789 & -1.6446 & -0.9973 & 0.3099 & 0 \\ 1.1379 & 1.7484 & -0.4261 & 1.1098 & 0 \end{bmatrix}.$$

By setting $\iota = 1$, one obtains the trajectories of leaders from (40). Moreover, the upper bounds of $\dot{\boldsymbol{x}}^*(t)$, $\dot{\boldsymbol{y}}^*(t)$, and $\dot{\boldsymbol{p}}_s(t)$, $s \in \boldsymbol{\mathcal{V}}_l$ is also obtained.

Then, the parameters for the shape estimator (13), translation estimator (27), and formation tracking controller (33) and (41) are select as follows satisfying Assumptions 5-7.

$$\alpha = 3, \quad \gamma_i = 3, \quad k = 2,$$

$$\sigma_1 = 1, \quad \sigma_2 = 2, \quad \sigma_3 = 2, \quad \rho = 2.$$

B. Simulation Results

Fig. 5 and Fig. 6 illustrate that linear formation shape and translation estimation errors all converge to zero. It validates the effectiveness of the proposed shape and translation estimators (13) and (27). The formation tracking errors are presented in Fig. 7. One observes that the convergence of formation tracking errors is slower than estimation errors shown in Fig. 5 and 6, as we can see that estimation errors converge within 2s but formation tracking errors take longer. This phenomenon also confirms the cascaded relationship between the proposed estimators and controllers. Additionally, within 10s, the formation tracking errors converge to a very small value. It guarantees the safety of subsequent obstacle avoidance maneuvers, as we can see the translational maneuver begins at 10s (also see the given reference translation parameter $\dot{\boldsymbol{y}}^{\mathrm{ref}} = \boldsymbol{0}_2$, $t < 10s$).

Fig. 8 shows the entire process of the formation maneuver task in the environment with obstacles. The maneuver task involves passing through a narrow passage between two obstacles. Before 10s, agents identify formation shape and translation parameters, waiting for the formation tracking errors to converge to sufficiently small values. Then, they maneuver in the $x+$ direction and shrink the formation (10s - 45s). Next, the team's formation compresses in y axis to cross the narrow passage between two obstacles (45s - 75s). After exiting the obstacle area, the compressed formation begins to recover (75s - 105s). Finally, the group of agents reaches the destination $\begin{bmatrix} 0 & 40 \end{bmatrix}$m, and forms the reference target formation in 150s. Throughout the whole maneuvering process, a flexible formation maneuver is realized based on the proposed time-varying linear formation control schemes.

VIII. Conclusion

We have proposed a time-varying linear formation control architecture for multi-agent systems. This architecture offers a

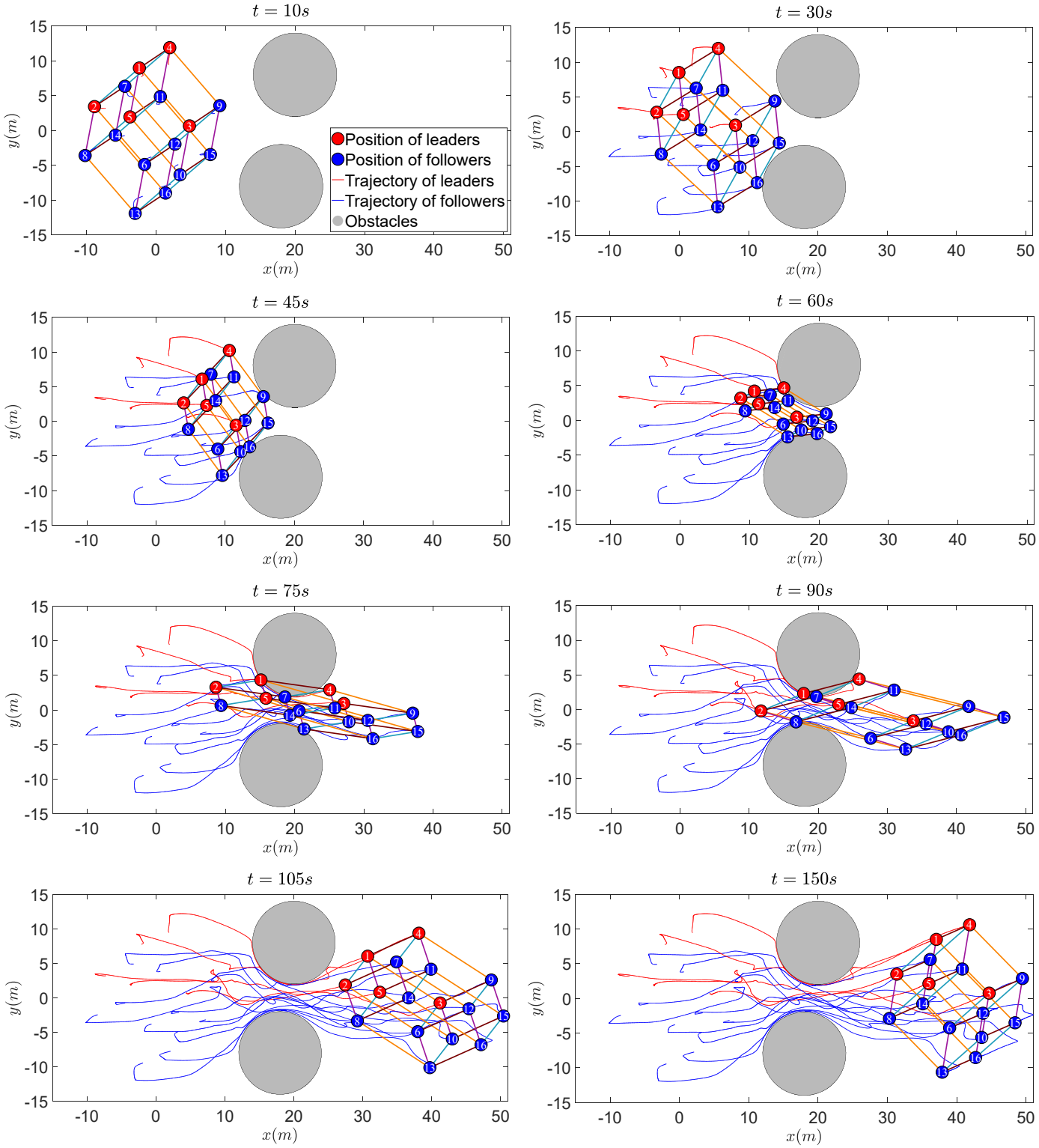

Fig. 8. Formation variations in the simulation. Note that straight lines connecting two agents in this figure do not represent a connected topology, but only represent edges that are parallel to the 4 coordinate axes in the nominal formation, given in Fig. 4.

broad set of flexible formations by specifying a time-varying nominal configuration that can lie in a higher-dimensional space than the agents' workspace.

An estimation-based formation control scheme has been proposed for time-varying formation tracking. One impressive thing is that the proposed control schemes allow the challenge case that the nominal configuration is time-varying. Estimators have been proposed to obtain precise time-varying shape and translation parameters, from the observation of leaders' motion. Furthermore, the proposed estimator essentially also accomplishes the problem of distributed solving a system of time-varying linear equations. Based on these estimation results, the time-varying linear formation tracking controller has been given to enhance formation maneuverability in complex environments.

In future research, there are several interesting topics, including nonlinear formation transformation, distributed linear formation parameter decision, and uncertainties in linear formation identification.

APPENDIX

A. Time-varying Linear Formation Design

This subsection describes a time-varying target formation design method. In light of Theorem 1, under Assumption 3, we know that the target formation is uniquely determined by leaders. The linear formation parameters can be expressed through the desired positions of leaders as follows:

$$\mathrm{vec}(\bar{\mathbf{A}}(t)) = (\bar{\mathbf{R}}_l^{+}(t) \otimes \mathbf{I}_d)\boldsymbol{p}_l^*(t).$$

Therefore, notice that linear formation design is essentially the desired trajectory planning of leaders. The desired position of followers is represented by that of leaders, i.e.,

$$\begin{aligned}\boldsymbol{p}_i^*(t) &= (\bar{\boldsymbol{r}}_i(t) \otimes \mathbf{I}_d)\,\mathrm{vec}(\bar{\mathbf{A}}(t)) \\ &= (\bar{\boldsymbol{r}}_i(t) \otimes \mathbf{I}_d)\,(\bar{\mathbf{R}}_l^{+}(t) \otimes \mathbf{I}_d)\boldsymbol{p}_l^*(t) \\ &= \mathbf{G}_i(\boldsymbol{r}_i(t))\boldsymbol{p}_l^*(t) \\ &= \sum_{j\in\boldsymbol{\mathcal{V}}_l} \mathbf{G}_{ij}(t)\boldsymbol{p}_j^*(t),\end{aligned}$$

where

$$\begin{aligned}\mathbf{G}_i(\boldsymbol{r}_i(t)) &= \left[\begin{array}{c|c|c} \mathbf{G}_{i1}(t) & \ldots & \mathbf{G}_{in_l}(t) \end{array}\right] \\ &= (\bar{\boldsymbol{r}}_i(t) \otimes \mathbf{I}_d)\,(\bar{\mathbf{R}}_l^{+}(t) \otimes \mathbf{I}_d).\end{aligned}$$

There are n_o environmental obstacles. The formation optimization is formulated as follows:

$$\begin{cases} \min \;\; J_1(t) \\ s.t. \;\; h_{ik}\left(t,\boldsymbol{p}_i^*,\boldsymbol{q}_k\right) \le 0 \quad i\in\boldsymbol{\mathcal{V}}, k=1,...,n_o\,, \\ \quad\;\; w_{ij}\left(t,\boldsymbol{p}_i^*,\boldsymbol{p}_j^*\right) \le 0 \quad i,j\in\boldsymbol{\mathcal{V}}, i\neq j \end{cases} \tag{38}$$

where $J_1(t)$ represents the formation keeping performance. $h_{ik}\left(t,\boldsymbol{p}_i^*,\boldsymbol{q}_k\right)$ represents the safe constraints for obstacle avoidance of agent i. $w_{ij}\left(t,\boldsymbol{p}_i^*,\boldsymbol{p}_j^*\right)$ represents reciprocal avoidance constraints between agents i and j. The expressions of $J_1(t)$, $h_{ik}\left(t,\boldsymbol{p}_i^*,\boldsymbol{q}_k\right)$, and $w_{ik}\left(t,\boldsymbol{p}_i^*,\boldsymbol{p}_j^*\right)$ is designed as

$$\begin{aligned}J_1(t) =& \mathrm{vec}\left(\tilde{\mathbf{A}}(t)\right)^{\mathrm{T}}\mathbf{Q}\mathrm{vec}\left(\tilde{\mathbf{A}}(t)\right), \\ \mathrm{vec}\left(\tilde{\mathbf{A}}(t)\right) =& \mathrm{vec}\left(\bar{\mathbf{A}}(t)\right) - \mathrm{vec}\left(\bar{\mathbf{A}}^{\mathrm{ref}}(t)\right)\end{aligned}$$

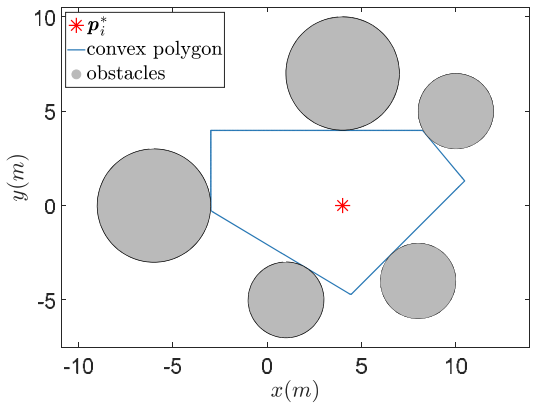

Fig. 9. The convex polygon constructed from obstacles.

$$\begin{aligned}h_{ik}\left(t,\boldsymbol{p}_i^*,\boldsymbol{q}_k\right) =& l_k\left[\left(\boldsymbol{p}_i^*(t)-\boldsymbol{q}_k(t)\right)^{\mathrm{T}}\left(\boldsymbol{p}_i^*(t)-\boldsymbol{q}_k(t)\right)\right]^{\frac{1}{2}} \\ &-\left(\boldsymbol{p}_i^*(t)-\boldsymbol{q}_k(t)\right)^{\mathrm{T}}\left(\boldsymbol{p}_i^*(t)-\boldsymbol{q}_k(t)\right), \\ w_{ij}\left(t,\boldsymbol{p}_i^*,\boldsymbol{p}_j^*\right) =& l\left[\left(\boldsymbol{p}_i^*(t)-\boldsymbol{p}_j^*(t)\right)^{\mathrm{T}}\left(\boldsymbol{p}_i^*(t)-\boldsymbol{p}_j^*(t)\right)\right]^{\frac{1}{2}} \\ &-\left(\boldsymbol{p}_i^*(t)-\boldsymbol{p}_j^*(t)\right)^{\mathrm{T}}\left(\boldsymbol{p}_i^*(t)-\boldsymbol{p}_j^*(t)\right),\end{aligned}$$

where $\mathbf{Q}$ is a diagonally positive definite coefficient matrix; $\mathrm{vec}\left(\bar{\mathbf{A}}^{\mathrm{ref}}(t)\right)$ is a predefined time-varying reference linear formation transformation matrix; $\boldsymbol{q}_k(t)$ represents the position of obstacle k. l_k and l denote safe distances; $h_{ik}\left(t,\boldsymbol{p}_i^*,\boldsymbol{q}_k\right)$ and $w_{ij}\left(t,\boldsymbol{p}_i^*,\boldsymbol{q}_k\right)$ are constructed from the point-normal form of lines. For example, Fig. 9 illustrates an example of the resulted convex polygon from constraints $\{h_{ik}\left(t,\boldsymbol{p}_i^*,\boldsymbol{q}_k\right)\}_{k=1}^{n_o}$.

By using interior point method [51], the constrained optimization (38) is reformulated into the following unconstrained optimization:

$$\min \;\; J_1(t) + J_2(t) + J_3(t), \tag{39}$$

where

$$\begin{aligned}J_2(t) &= -\frac{1}{t+1}\left[\sum_{i=1}^{n}\sum_{k=1}^{m}\ln\left(-h_{ik}\left(t,\boldsymbol{p}_i^*,\boldsymbol{q}_k^*\right)\right)\right], \\ J_3(t) &= -\frac{1}{t+1}\left[\sum_{i=1}^{n}\sum_{j=i+1}^{n}\ln\left(-w_{ij}\left(t,\boldsymbol{p}_i^*,\boldsymbol{p}_j^*\right)\right)\right].\end{aligned}$$

J_2 is derived from constraints $h_{ik}\left(t,\boldsymbol{p}_i^*,\boldsymbol{q}_k\right) \le 0$; J_3 is derived from constraints $w_{ij}\left(t,\boldsymbol{p}_i^*,\boldsymbol{q}_k\right) \le 0$. Since $h_{ik} \le 0$ is non-convex, (39) is also a non-convex optimization. However, feasible desired trajectories for leaders can be obtained by enforcing $\boldsymbol{p}_l^*(t)$ to move along the gradient descent direction of $J(t) \triangleq J_1(t) + J_2(t) + J_3(t)$, as expressed by

$$\dot{\boldsymbol{p}}_s^*(t) = -\left(\iota\nabla_{\boldsymbol{p}_s^*}J(t) + \frac{\partial}{\partial t}\nabla_{\boldsymbol{p}_s^*}J(t)\right), \quad \forall s\in\boldsymbol{\mathcal{V}}_l, \tag{40}$$

where $\iota > 0$.

In addition, leaders can employ the following tracking controller to track the obtained desired trajectory:

$$\boldsymbol{u}_i(t) = \dot{\boldsymbol{p}}_i^*(t) - \rho\left(\boldsymbol{p}_i(t) - \boldsymbol{p}_i^*(t)\right), \qquad \forall i\in\boldsymbol{\mathcal{V}}_l. \tag{41}$$

B. Proof of Lemma 5

Form the definition of $\mathbf{\Pi}_i(t)$ (below (15)), one knows $\mathbf{I}_{df} - \mathbf{\Pi}_i(t)$ is a positive (semi-)definite matrix when $i \in \boldsymbol{\mathcal{V}}_{f1}$, and null matrix when $i \in \boldsymbol{\mathcal{V}}_{f2}$. From the fact that $\boldsymbol{\mathcal{V}}_{f1} \neq \varnothing$, it is conducted that $\mathbf{I}_{df n_f} - \mathbf{\Pi}(t)$ is positive semi-definite. In view of Assumption 1, it is obtained that $\bar{\boldsymbol{\mathcal{L}}}_f$ is also positive semi-definite. Thus, in order to prove Lemma 3, it is sufficient to establish that $\left(\mathbf{I}_{df n_f} - \mathbf{\Pi}(t)\right) + \bar{\boldsymbol{\mathcal{L}}}_f$ is non-singular, which will be proven by assuming the contrary to obtain a contradiction.

Suppose there is a nonzero vector $\boldsymbol{\psi}(t) \in \mathbb{R}^{df n_f}$ satisfying $\left[\left(\mathbf{I}_{df n_f} - \mathbf{\Pi}(t)\right) + \bar{\boldsymbol{\mathcal{L}}}_f\right] \boldsymbol{\psi}(t) = \boldsymbol{0}_{df n_f}$. Then, it clearly has

$$\begin{aligned} \left(\mathbf{I}_{df n_f} - \mathbf{\Pi}(t)\right) \boldsymbol{\psi}(t) &= \boldsymbol{0}_{df n_f}, \\ \bar{\boldsymbol{\mathcal{L}}}_f \boldsymbol{\psi}(t) &= \boldsymbol{0}_{df n_f}. \end{aligned}$$

In view of $\bar{\boldsymbol{\mathcal{L}}}_f \boldsymbol{\psi}(t) = \boldsymbol{0}_{df n_f}$, $\boldsymbol{\psi}$ can be denoted by $\boldsymbol{\psi}(t) = \boldsymbol{1}_{n_f} \otimes \boldsymbol{\theta}(t)$, $\boldsymbol{\theta}(t) \in \mathbb{R}^{df}$. Then, from $\left(\mathbf{I}_{df n_f} - \mathbf{\Pi}(t)\right) \boldsymbol{\psi}(t) = \boldsymbol{0}_{df n_f}$, we obtain $\mathbf{M}_i(t)\boldsymbol{\theta}(t) = \boldsymbol{0}_{df}$, $\forall i \in \boldsymbol{\mathcal{V}}_{f1}$. For all followers belonging to $\boldsymbol{\mathcal{V}}_{f1}$, they establish the following system of linear equations:

$$\mathbf{M}_f(t)\hat{\boldsymbol{\theta}}(t) = \boldsymbol{0}_m, \tag{42}$$

where

$$\begin{aligned} \mathbf{M}_f(t) &= \begin{bmatrix} \cdots & \mathbf{M}_i{}^{\mathrm{T}}(t) & \cdots \end{bmatrix}^{\mathrm{T}}, \quad i \in \boldsymbol{\mathcal{V}}_{f1}, \\ \hat{\boldsymbol{\theta}}(t) &= \boldsymbol{1}_{|\boldsymbol{\mathcal{V}}_{f1}|} \otimes \boldsymbol{\theta}(t). \end{aligned}$$

According to Assumption 4, the measurable leaders' edge displacements linearly span $\mathbb{R}^f$ in the nominal configuration. Therefore, $\operatorname{rank}\left(\mathbf{M}_f(t)\right) \equiv \operatorname{rank}\left(\begin{bmatrix}\mathbf{M}_f(t) & \boldsymbol{0}\end{bmatrix}\right) \equiv df$. In view of Section II-C, (42) has the unique solution $\hat{\boldsymbol{\theta}}(t) = \boldsymbol{0}_{|\boldsymbol{\mathcal{V}}_{f1}|df}$, which implies $\boldsymbol{\theta}(t) = \boldsymbol{0}_{df}$. Thus, we obtain $\boldsymbol{\psi}(t) = \boldsymbol{0}_{n_f df}$. This contradicts the hypothesis.

Hence, $\left(\mathbf{I}_{df n_f} - \mathbf{\Pi}(t)\right) + \bar{\boldsymbol{\mathcal{L}}}_f$ is non-singular, and thus positive definite.

REFERENCES

[1] A. Franchi, P. Stegagno, and G. Oriolo, "Decentralized multi-robot encirclement of a 3D target with guaranteed collision avoidance," *Auton. Robots*, vol. 40, no. 2, pp. 245-265, Feb. 2016.

[2] Y. Liu, F. Zhang, P. Huang, and Y. Lu, "Configuration Optimization and Distributed Formation Control for Tethered Multirotor UAS," *IEEE/ASME Trans. Mechatronics*, vol. 28, no. 6, pp. 3434-3445, Dec. 2023.

[3] X. Zhang, F. Zhang, and P. Huang, "Formation Planning for Tethered Multirotor UAV Cooperative Transportation With Unknown Payload and Cable Length," *IEEE Trans. Autom. Sci. Eng.*, vol. 21, no. 3, pp. 3449-3460, Jul. 2024.

[4] C. Zhang, N. Noguchi, and L. Yang, "Leader-follower system using two robot tractors to improve work efficiency," *Comput. Electron. Agric.*, vol. 121, pp. 269-281, Feb. 2016.

[5] C. A. Hirst, J. Burger, H. Havenga, G. Botha, D. Baumgardner, T. DeFelice, D. Axisa, and E. Frew, "An Autonomous Uncrewed Aircraft System Performing Targeted Atmospheric Observation for Cloud Seeding Operations," *F. Robot.*, vol. 3, no. 1, pp. 687-724, Jan. 2023.

[6] R. Olfati-Saber, J. A. Fax, and R. M. Murray, "Consensus and cooperation in networked multi-agent systems," *Proc. IEEE*, vol. 95, no. 1, pp. 215-233, Jan. 2007.

[7] W. Ren and E. Atkins, "Distributed multi-vehicle coordinated controlvia local information exchange," *Int. J. Robust Nonlinear Control*, vol. 17, no. 10-11, pp. 1002-1033, Jul. 2007.

[8] W. Ren and N. Sorensen, "Distributed coordination architecture for multi-robot formation control," *Rob. Auton. Syst.*, vol. 56, no. 4, pp. 324-333, Apr. 2008.

[9] S. Coogan and M. Arcak, "Scaling the size of a formation using relative position feedback," *Automatica*, vol. 48, no. 10, pp. 2677-2685, Oct. 2012.

[10] S. Zhao and D. Zelazo, "Translational and scaling formation maneuver control via a bearing-based approach," *IEEE Trans. Control Netw. Syst.*, vol. 4, no. 3, pp. 429-438, Sep. 2017.

[11] I. Buckley and M. Egerstedt, "Infinitesimal Shape-Similarity for Characterization and Control of Bearing-Only Multirobot Formations," *IEEE Trans. Robot.*, vol. 37, no. 6, pp. 1921-1935, Dec. 2021.

[12] L. Chen, Q. Yang, M. Shi, Y. Li, and M. Feroskhan, "Stabilizing Angle Rigid Formations With Prescribed Orientation and Scale," *IEEE Trans. Ind. Electron.*, vol. 69, no. 11, pp. 11654-11664, Nov. 2022.

[13] Z. Lin, L. Wang, Z. Chen, M. Fu, and Z. Han, "Necessary and Sufficient Graphical Conditions for Affine Formation Control," *IEEE Trans. Automat. Contr.*, vol. 61, no. 10, pp. 2877-2891, Oct. 2016.

[14] S. Zhao, "Affine Formation Maneuver Control of Multiagent Systems," *IEEE Trans. Automat. Contr.*, vol. 63, no. 12, pp. 4140-4155, Dec. 2018.

[15] Y. Lin, Z. Lin, Z. Sun, and B. D. O. Anderson, "A Unified Approach for Finite-Time Global Stabilization of Affine, Rigid, and Translational Formation," *IEEE Trans. Automat. Contr.*, vol. 67, no. 4, pp. 1869-1881, Apr. 2022.

[16] Q. Yang, H. Fang, M. Cao, and J. Chen, "Planar Affine Formation Stabilization via Parameter Estimations," *IEEE Trans. Cybern.*, vol. 52, no. 6, pp. 5322-5332, Jun. 2022.

[17] X. Dong, B. Yu, Z. Shi, and Y. Zhong, "Time-varying formation control for unmanned aerial vehicles: Theories and applications," *IEEE Trans. Control Syst. Technol.*, vol. 23, no. 1, pp. 340-348, Jan. 2015.

[18] X. Zhang, Q. Yang, J. Lyu, X. Zhao, and H. Fang, "Distributed Variation Parameter Design for Dynamic Formation Maneuvers With Bearing Constraints," *IEEE Trans. Autom. Sci. Eng.*, vol. 21, no. 3, pp. 3664-3677, 2024.

[19] J. Yu, X. Dong, Q. Li, and Z. Ren, "Practical Time-Varying Formation Tracking for Second-Order Nonlinear Multiagent Systems With Multiple Leaders Using Adaptive Neural Networks," *IEEE Trans. Neural Networks Learn. Syst.*, vol. 29, no. 12, pp. 6015-6025, Dec. 2018.

[20] J. Pan, T. Han, B. Xiao, X. S. Zhan, and H. Yan, "Predefined-Time Bipartite Time-Varying Formation Tracking of Multiple Euler-Lagrange Systems Via Estimator-Based Hierarchical Control Algorithm," *IEEE Trans. Circuits Syst. II Express Briefs*, vol. 70, no. 9, pp. 3444-3448, Sep. 2023.

[21] Y. Ren, K. Zhang, B. Jiang, W. Cheng, and Y. Ding, "Distributed fault-tolerant time-varying formation control of heterogeneous multi-agent systems," *Int. J. Robust Nonlinear Control*, vol. 32, no. 5, pp. 2864-2882, Mar. 2022.

[22] H. Garcia de Marina, "Distributed formation maneuver control by manipulating the complex Laplacian," *Automatica*, vol. 132, p. 109813, Oct. 2021.

[23] J. Wang, X. Ding, C. Wang, Z. Zuo, and Z. Ding, "Affine Formation Control of General Linear Multi-Agent Systems with Delays," *Unmanned Syst.*, vol. 11, no. 02, pp. 123-132, Apr. 2023.

[24] Y. Xu, S. Zhao, D. Luo, and Y. You, "Affine formation maneuver control of high-order multi-agent systems over directed networks," *Automatica*, vol. 118, p. 109004, Aug. 2020.

[25] O. Onuoha, H. Tnunay, Z. Li, and Z. Ding, "Affine Formation Algorithms and Implementation Based on Triple-Integrator Dynamics," *Unmanned Syst.*, vol. 07, no. 01, pp. 33-45, Jan. 2019.

[26] W. Yu, B. Zhu, X. Wang, P. Yi, H. Liu, and T. Hu, "Enhanced Affine Formation Maneuver Control Using Historical Velocity Command (HVC)," *IEEE Robot. Autom. Lett.*, vol. 8, no. 11, pp. 7186-7193, Nov. 2023.

[27] L. Chen, J. Mei, C. Li, and G. Ma, "Distributed Leader-Follower Affine Formation Maneuver Control for High-Order Multiagent Systems," *IEEE Trans. Automat. Contr.*, vol. 65, no. 11, pp. 4941-4948, Nov. 2020.

[28] Z. Miao, Y. H. Liu, Y. Wang, G. Yi, and R. Fierro, "Distributed Estimation and Control for Leader-Following Formations of Nonholonomic Mobile Robots," *IEEE Trans. Autom. Sci. Eng.*, vol. 15, no. 4, pp. 1946-1954, Oct. 2018.

[29] Q. Yang, Z. Sun, M. Cao, H. Fang, and J. Chen, "Stress-matrix-based formation scaling control," *Automatica*, vol. 101, pp. 120-127, Mar. 2019.

[30] Y. Liu, Z. Ma, F. Zhang, and P. Huang, "Time-Varying Formation Planning and Scaling Control for Tethered Space Net Robot," *IEEE Trans. Aerosp. Electron. Syst.*, vol. 59, no. 5, pp. 1–12, 2023.

[31] S. Mou, J. Liu, and A. S. Morse, "A Distributed Algorithm for Solving a Linear Algebraic Equation," *IEEE Trans. Automat. Contr.*, vol. 60, no. 11, pp. 2863-2878, Nov. 2015.

[32] B. Anderson, S. Mou, A. Morse, and U. Helmke, "Decentralized gradient algorithm for solution of a linear equation," *Numer. Algebr. Control Optim.*, vol. 6, no. 3, pp. 319-328, Sep. 2016.
[33] J. Liu, A. Stephen Morse, A. Nedić, and T. Başar, "Exponential convergence of a distributed algorithm for solving linear algebraic equations," *Automatica*, vol. 83, pp. 37-46, Sep. 2017.
[34] S. S. Alaviani and N. Elia, "A Distributed Algorithm for Solving Linear Algebraic Equations over Random Networks," *IEEE Trans. Automat. Contr.*, vol. 66, no. 5, pp. 2399-2406, May 2021.
[35] X. Wang, S. Mou, and D. Sun, "Improvement of a Distributed Algorithm for Solving Linear Equations," *IEEE Trans. Ind. Electron.*, vol. 64, no. 4, pp. 3113-3117, Apr. 2017.
[36] J. Zhou, X. Wang, S. Mou, and B. D. O. Anderson, "Finite-Time Distributed Linear Equation Solver for Solutions with Minimum l_1-Norm," *IEEE Trans. Automat. Contr.*, vol. 65, no. 4, pp. 1691-1696, Apr. 2020.
[37] X. Wang, J. Zhou, S. Mou, and M. J. Corless, "A distributed algorithm for least squares solutions," *IEEE Trans. Automat. Contr.*, vol. 64, no. 10, pp. 4217-4222, 2019.
[38] G. Shi, B. D. O. Anderson, and U. Helmke, "Network Flows That Solve Linear Equations," *IEEE Trans. Automat. Contr.*, vol. 62, no. 6, pp. 2659-2674, Jun. 2017.
[39] Y. Liu, C. Lageman, B. D. O. Anderson, and G. Shi, "An Arrow-Hurwicz-Uzawa type flow as least squares solver for network linear equations," *Automatica*, vol. 100, pp. 187-193, Feb. 2019.
[40] X. Zhang, Q. Yang, H. Wei, W. Chen, Z. Peng, and H. Fang, "A Distributed Algorithm for Solving A Time-Varying Linear Equation," in *Proc. IEEE Conf. Decis. Control (CDC)*, Dec. 2023, pp. 3160-3165.
[41] R. A. Horn and C.R. Johnson, *Matrix Analysis 2nd Edition*, 2012.
[42] C. Godsil and G. Royle, *Algebraic Graph Theory*, 2001.
[43] T. Opsahl and P. Panzarasa, "Clustering in weighted networks," *Soc. Networks*, vol. 31, no. 2, pp. 155-163, May 2009.
[44] D. C. Lay, S. R. Lay, and J. J. McDonald, *Linear Algebra and Its Applications 5th Edition*, 2014.
[45] J. Cortés, "Discontinuous dynamical systems," *IEEE Control Syst.*, vol. 28, no. 3, pp. 36-73, Jun. 2008.
[46] S. Yu, X. Yu, B. Shirinzadeh, and Z. Man, "Continuous finite-time control for robotic manipulators with terminal sliding mode," *Automatica*, vol. 41, no. 11, pp. 1957-1964, Nov. 2005.
[47] S. P. Bhat and D. S. Bernstein, "Finite-Time Stability of Continuous Autonomous Systems," *SIAM J. Control Optim.*, vol. 38, no. 3, pp. 751-766, Jan. 2000.
[48] M. Maggiore, A. Loría, and E. Panteley, "Reduction theorems for stability of compact sets in time-varying systems," *Automatica*, vol. 148, p. 110771, Feb. 2023.
[49] S. Li and Y. P. Tian, "Finite-time stability of cascaded time-varying systems," *Int. J. Control*, vol. 80, no. 4, pp. 646-657, Apr. 2007.
[50] X. Zhang, Q. Yang, F. Xiao, H. Fang, and J. Chen, "Linear formation control of multi-agent systems," *Automatica*, vol. 171, p. 111935, Jan. 2025.
[51] F. A. Potra and S. J. Wright, "Interior-point methods," *J. Comput. Appl. Math.*, vol. 124, no. 1, pp. 281-302, Dec. 2000.

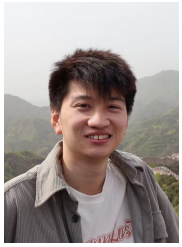

Xiaozhen Zhang received M.S. degree in navigation, guidance and control, from Northwestern Polytechnical University, Xi'an, China, in 2021. He is currently working toward the Ph.D. degree in control engineering at Beijing Institute of Technology, Beijing, China.

His research interests include multi-agent systems, networked control, and swarm robotics.

Qingkai Yang (Member, IEEE) received the first Ph.D. degree in control science and engineering from the Beijing Institute of Technology, Beijing, China, in 2018, and the second Ph.D. degree in system control from the University of Groningen, Groningen, The Netherlands, in 2018. He is currently a Professor with the School of Automation, Beijing Institute of Technology.

His research interests include cooperative control of multi-agent systems, autonomous mobile robots, and swarm intelligence.

Xianlin Zeng (Member, IEEE) received the B.S. and M.S. degrees in Control Science and Engineering from the Harbin Institute of Technology, Harbin, China, in 2009 and 2011, respectively, and the Ph.D. degree in Mechanical Engineering from the Texas Tech University in 2015. He is currently a Professor in the Key Laboratory of Autonomous Intelligent Unmanned Systems, School of Automation, Beijing Institute of Technology, Beijing, China. His current research interests include distributed optimization, distributed control, and distributed computation of network systems.

Hao Fang (Member, IEEE) received the B.S. degree from the Xi'an University of Technology, Shaanxi, China, in 1995, and the M.S. and Ph.D. degrees from the Xi'an Jiaotong University, Shaanxi, in 1998 and 2002, respectively.

Since 2011, he has been a Professor with the Beijing Institute of Technology, Beijing, China. He held two postdoctoral appointments with the INRIA/France Research Group of COPRIN and the LASMEA (UNR6602 CNRS/Blaise Pascal University, Clermont-Ferrand, France).

His research interests include all-terrain mobile robots, robotic control, and multiagent systems.

Jie Chen (Fellow, IEEE) received his B.Sc., M.Sc., and the Ph.D. degrees in Control Theory and Control Engineering from the Beijing Institute of Technology, Beijing, China, in 1986, 1996, and 2001, respectively. He was the President of Tongji University, Shanghai, China, during 2018-2023. He is a Professor with the Control Science and Engineering, Beijing Institute of Technology and Tongji University, where he serves as the Director of the National Key Laboratory of Autonomous Intelligent Unmanned Systems (KAIUS).

His research interests include complex systems, multi-agent systems, multi-objective optimization and decision, and constrained nonlinear control. Prof. Chen is currently the Editor-in-Chief of Unmanned Systems and the Journal of Systems Science and Complexity. He has served on the editorial boards of several journals, including the IEEE Transactions on Cybernetics, International Journal of Robust and Nonlinear Control, and Science China Information Sciences. He is a Fellow of IEEE, IFAC, and a member of the Chinese Academy of Engineering.